The regulation of HAD-like phosphatases by signaling pathways modulates cellular resistance to the metabolic inhibitor, 2-deoxyglucose

Quentin Defenouillère, Agathe Verraes, Clotilde Laussel, Anne Friedrich, Joseph Schacherer, Sébastien Léon

The induction of HAD-like phosphatases by multiple signaling pathways confers resistance to the metabolic inhibitor 2-deoxyglucose

Quentin Defenouillère[1,2], Agathe Verraes[1,2], Clotilde Laussel[1], Anne Friedrich[3], Joseph Schacherer[3] & Sébastien Léon[1,4]

1: Institut Jacques Monod, UMR 7592 Centre National de la Recherche Scientifique/Université Paris-Diderot, Sorbonne Paris Cité, 75205 Paris cedex 13, France

2: These authors contributed equally to this work

3: Université de Strasbourg, CNRS, GMGM UMR 7156, 67000 Strasbourg, France

4: Author for correspondence:

Sébastien Léon, PhD

Institut Jacques Monod

15 Rue Hélène Brion

75205 Paris Cedex 13, France.

email: sebastien.leon@ijm.fr; tel. +33 (0)1 57 27 80 57.

Abstract

Anti-cancer strategies that target the glycolytic metabolism of tumors have been proposed. The glucose analog 2-deoxyglucose (2DG) is imported into cells and after phosphorylation becomes 2DG-6-phosphate, a toxic by-product that inhibits glycolysis. Using yeast as a model, we performed an unbiased mass spectrometry-based approach to probe the cellular effects of 2DG on the proteome and study resistance mechanisms to 2DG. We found that two phosphatases that target 2DG-6-phosphate were induced upon exposure to 2DG and participated in 2DG detoxication. Dog1 and Dog2 are HAD (haloacid dehalogenase)-like phosphatases, which are evolutionarily conserved. 2DG induced Dog2 by activating several signaling pathways, such as the stress response pathway mediated by the p38 MAPK ortholog Hog1, the unfolded protein response (UPR) triggered by 2DG-induced ER stress, and the cell wall integrity (CWI) pathway mediated by the MAPK Slt2. Loss of the UPR or CWI pathways led to 2DG hypersensitivity. In contrast, mutants impaired in the glucose-mediated repression of genes, were 2DG-resistant because glucose availability transcriptionally repressed *DOG2* by inhibiting signaling mediated by the AMPK ortholog Snf1. The characterization and genome resequencing of spontaneous 2DG-resistant mutants revealed that *DOG2* overexpression was a common strategy underlying 2DG resistance. The human Dog2 homolog HDHD1 displayed 2DG-6-phosphate phosphatase activity in vitro and its overexpression conferred 2DG resistance in HeLa cells, suggesting that this 2DG phosphatase could interfere with 2DG-based chemotherapies. These results show that HAD-like phosphatases are evolutionarily conserved regulators of 2DG resistance.

Introduction

Most cancer cells display an altered metabolism, with an increased glucose consumption to support their proliferative metabolism that is based on aerobic glycolysis (Warburg effect) (*1, 2*). Inhibiting glycolysis has been proposed as a strategy to target cancer cells and various metabolic inhibitors have been considered (*3, 4*).

2-deoxy-D-glucose (2DG) is a derivative of D-glucose that is imported by glucose transporters and is phosphorylated by hexokinase into 2-deoxy-D-glucose-6-phosphate (2DG6P), but cannot be further metabolized due to the 2-deoxy substitution, triggering a decrease in cellular ATP content in tumors (*5*). Mechanistically, 2DG6P accumulation hampers glycolysis by inhibiting hexokinase activity in a non-competitive manner (*6, 7*), as well as by inhibiting phospho-glucose isomerase activity in a competitive manner (*8*). Because cancer cells rely on an increased glycolysis rate for proliferation, 2DG has been of interest for cancer therapy, particularly in combination with radiotherapy or other metabolic inhibitors (*9-11*). These features led to a phase I clinical trial using 2DG in combination with other drugs to treat solid tumors (*12*). Its derivative ^{18}Fluoro-2DG is also used in cancer imaging (PET scans) because it preferentially accumulates in tumor cells due to their increased glucose uptake (*13*). Additionally, due to its structural similarity to mannose, 2DG (which could also be referred as to 2-deoxymannose, because mannose is the C2 epimer of glucose) also interferes with N-linked glycosylation and causes ER stress (*14-16*), which has been proposed to be the main mechanism by which 2DG kills normoxic cells (*17*). 2DG toxicity has also been linked to the depletion of phosphate pools following 2DG phosphorylation (*18*). Finally, interference of 2DG with lipid metabolism and calcium homeostasis through unknown underlying mechanisms have been described (*19*). Resistance to 2-deoxyglucose has been detected in cell cultures (*20*).

Because these metabolic and signalling pathways are evolutionarily conserved, simpler eukaryotic models such as the budding yeast *Saccharomyces cerevisiae* can be used to understand the mode of action of 2DG. Moreover, yeast is particularly well-suited for these studies because of its peculiar metabolism (*21*). Akin to cancer cells, *Saccharomyces cerevisiae* preferentially consumes

glucose through glycolysis over respiration, regardless of the presence of oxygen. This occurs through glucose-mediated repression of genes involved in respiration and alternative carbon metabolism, which operates at the transcriptional level. This glucose-mediated repression mechanism is relieved upon activation of the yeast ortholog of 5'AMP-activated protein kinase (AMPK), Snf1, which phosphorylates the transcriptional repressor Mig1 and leads to its translocation out of the nucleus (*22-25*). Mutations that render yeast cells more tolerant to 2DG have been identified (*26-31*). These findings suggest the existence of cellular mechanisms that can modulate 2DG toxicity, which are important to characterize if 2DG is to be used therapeutically.

In yeast, 2DG was initially used to identify genes involved in glucose repression because 2DG, like glucose, causes Snf1 inactivation and thus prevents the use of alternative carbon sources (*32-34*). The characterization of mutants that can grow in 2DG-containing sucrose medium has allowed the identification of components of the glucose repression pathway (*26, 29, 35*) and has revealed that mutations in *HXK2,* which encodes hexokinase II, also render yeast cells more tolerant to 2DG, perhaps by limiting 2DG phosphorylation and 2DG6P accumulation (*29-31, 36, 37*). Finally, several 2DG-resistant mutants display increased 2DG6P phosphatase activity, which could detoxify the cells of this metabolite and dampen its negative effects on cellular physiology (*38, 39*). Indeed, two 2DG6P phosphatases named *DOG1* and *DOG2* have been cloned, and their overexpression triggers 2DG resistance and prevents 2DG-mediated repression of genes (*33, 40, 41*).

The toxicity of 2DG has also been studied in the context of cells grown in glucose-containing media, which may be more relevant for the understanding its mode of action in mammalian cells. Under these conditions, 2DG toxicity is independent of its effect on the glucose repression of genes and involves different mechanisms, such as a direct inhibition of glycolysis and other cellular pathways (*30, 42, 43*). Accordingly, several mutations leading to 2DG resistance in cells grown in sucrose medium do not lead to resistance in cells grown in glucose medium (*30, 44*). Deletion of *REG1*, which encodes a regulatory subunit of protein phosphatase 1 (PP1) that inhibits Snf1 (*45, 46*) leads to 2DG resistance (*30*). The resistance of the *reg1Δ* mutant depends on the presence of Snf1, and the single deletion of

SNF1 also renders yeast hypersensitive to 2DG (*31*), thus demonstrating that Snf1 activity is crucial for 2DG resistance. A model has been proposed in which the 2DG sensitivity displayed by the *snf1*Δ mutant involves misregulated expression and localization of the low-affinity glucose transporters Hxt1 and Hxt3 (*47*). Additionally, the deletion of *LSM6*, which encodes a component of a complex involved in mRNA degradation, also leads to 2DG resistance in a Snf1-dependent manner, but the mechanism by which this occurs is unknown (*31*). Thus, many aspects of the pathways mediating 2DG sensitivity or resistance remain to be explored.

In the present study, our unbiased, mass-spectrometry-based approach in yeast revealed that the main 2DG6P phosphatase, Dog2, was induced upon exposure to 2DG and participated in 2DG detoxification in glucose medium. We found that 2DG induced Dog2 (and Dog1, to a certain extent), by triggering UPR and MAPK-based stress-responsive signaling pathways. Moreover, the expression of *DOG2* was additionally regulated by Snf1 and the glucose-repression pathway through the action of downstream transcriptional repressors and contributed to the resistance of glucose-repression mutants to 2DG. The partial characterization of 24 spontaneous 2DG-resistant mutants revealed that most mutants displayed increased *DOG2* expression, suggesting a common strategy used to acquire 2DG resistance. Particularly, genome resequencing identified that mutations in *CYC8*, which encodes a transcriptional corepressor, caused 2DG resistance through increased Dog2 expression. The identification of a potential human homolog of the Dog1/2 proteins, HDHD1, which displays 2-deoxyglucose-6-phosphate (2DG6P) phosphatase activity in vitro and which caused 2DG resistance in HeLa cells upon overexpression, suggests that HAD-like phosphatases are conserved regulators of 2DG resistance.

Results.

A proteomic assessment of the cellular response to 2DG reveals increased expression of metabolic enzymes

As a first step to characterize the cellular response of yeast cells to 2-deoxyglucose (2DG) treatment in an unbiased and quantitative manner, we performed proteome-wide mass spectrometry-based proteomics on WT cells treated with 0.2% 2DG, a concentration that prevents growth of WT cells on plates (*30*). Untreated cells were used as a negative control. Overall, 78 proteins were significantly more abundant, whereas 18 proteins were less abundant after 2DG treatment (False Discovery Rate (FDR) of 0.01) (**Fig. 1A, Data File S1**). Among the up-regulated candidates, proteins involved in various metabolic processes were significantly enriched, including those involved in the metabolism of glucose, glucose-6-phosphate and other carbohydrates (**Fig. 1B, fig. S1**), in line with 2DG interfering with glycolysis (*5*).

These proteomics data revealed an increase in the abundance of the 2-deoxyglucose-6-phosphate phosphatases Dog1 or Dog2, which could not be discriminated at the mass spectrometry level because of their high sequence identity (92%). Although these phosphatases can promote 2DG resistance (*33, 40, 41*), the increased expression of Dog1 and/or Dog2 in response to 2DG was intriguing because it raised the question of how exposure to this synthetic molecule could trigger an adaptive resistance mechanism in yeast. To first confirm that 2DG induced Dog1 and Dog2, we GFP-tagged each at their chromosomal locus to maintain endogenous regulation. Western blotting revealed that both Dog1 and Dog2 expression levels were increased in the presence of 2DG, and that Dog2-GFP was more abundant than Dog1-GFP (**Fig. 1C**).

To evaluate the contribution of transcription in the regulation of *DOG1* and *DOG2* genes by 2DG, we fused the corresponding promoters to a β-galactosidase reporter. 2DG increased the activity of the *DOG1* and *DOG2* promoters (**Fig. 1D**), suggesting that the expression of Dog1 and Dog2 was at least partially due to increased transcription. The deletion of *DOG2* sensitized yeast cells to 2DG, but that of *DOG1* had little effect (**Fig. 1E**), indicating that Dog2 is functionally more important than Dog1, perhaps

due to its higher expression level (Fig. 1C). These results indicate that Dog2 participates in the natural tolerance of WT cells to low concentrations (0.05%) of 2DG.

The expression of Dog2, whose endogenous function in yeast metabolism is unknown, is induced by various stresses, such as oxidative and osmotic stresses, through the stress-responsive mitogen activated protein kinase (MAPK) ortholog of p38, Hog1 (*48*). The deletion of *HOG1* prevented the maximal induction of *pDOG2*-LacZ expression (Fig. 1F) and Dog2 induction (Fig. 1G-H) without affecting the induction of Dog1 (fig. S2A). When we tested the effect of 2DG on Hog1 phosphorylation using an antibody directed against the phosphorylated form of mammalian p38 (*49*), we found that Hog1 appeared partially activated upon 2DG addition, but to a lower extent compared to the activation induced by hyperosmotic shock (fig. S2B). These data show that the stress-activated protein kinase Hog1 participates in Dog2 induction but also that the maximal expression of Dog1 and Dog2 by 2DG involves at least one additional level of regulation.

The expression of Dog1 and Dog2 is induced by the unfolded protein response pathway through 2DG-induced ER stress

Exposure of cancer cells to 2DG interferes with N-linked glycosylation, likely because of the structural similarity of 2DG with mannose, a constituent of the N-glycan structures (*14*). This interference results in endoplasmic reticulum (ER) stress and consequently, in the induction of the unfolded protein response (UPR) pathway in mammalian cells (*14*). Treatment of yeast with 2DG also induced a defect in the glycosylation of carboxypeptidase Y (CPY) (Fig. 2A), a vacuolar (lysosomal) protease whose membrane-anchored precursor is N-glycosylated in the course of its intracellular trafficking (*50*). This defect was not as extensive as that observed upon treatment of cells with tunicamycin, an inhibitor of the first step of glycosylation that also causes ER stress and is a strong UPR inducer (*51, 52*) (Fig. 2A). The addition of exogenous mannose in the medium suppressed the glycosylation defects caused by 2DG, but not those caused by tunicamycin (Fig. 2A). This result

supports the idea that 2DG mimics mannose and interferes with its incorporation in N-glycans, as has been proposed in mammalian cells (*14, 17*).

In yeast, the UPR pathway is initiated by a multifunctional ER membrane protein named Ire1. Upon sensing ER stress and after dimerization, Ire1 splices pre-mRNAs encoding the transcription factor Hac1, leading to its translation and the trans-activation of Hac1 targets carrying an UPRE (UPR Element) in their promoter (**Fig. 2B**) (*53*). To address whether 2DG can induce the UPR pathway in yeast, we used an UPRE-driven reporter, UPRE1-LacZ (*52*). 2DG elicited the expression of this reporter in a manner dependent on Hac1, confirming that 2DG is a bona fide UPR inducer (**Fig. 2C**).

We then tested whether 2DG-mediated induction of Dog2 involved the UPR pathway. First, we found that tunicamycin strongly induced the *pDOG2*-LacZ reporter (**Fig. 2D**), suggesting that glycosylation defects and/or the ensuing ER stress promotes *DOG2* expression. Moreover, the induction of this reporter by 2DG was reduced by more than 2-fold in *hac1Δ* mutant cells, suggesting that UPR contributed to this induction (**Fig. 2E**). Comparable results were obtained for p*DOG1*-LacZ (**fig. S3, A and B**). These results were confirmed at the protein level for Dog2 (**Fig. 2F-G**).

UPR-compromised mutants such as *hac1*Δ and *ire1*Δ were both hypersensitive to 2DG (**Fig. 2H**), suggesting that they cannot cope with ER stress caused by 2DG. The addition of exogenous mannose in the medium, which can alleviate the glycosylation defects caused by 2DG (**Fig. 2A**), restored 2DG-tolerance of these mutants to a comparable level as that of WT cells (**Fig. 2H**) but not that of *snf1*Δ, a 2DG-hypersensitive mutant (*31*). Together, these results confirm that 2DG induces ER stress by interfering with N-glycosylation, that the subsequent activation of the UPR pathway increased Dog1 and Dog2 expression, and that UPR mutants display an increased sensitivity to 2DG which correlates with a lower level of Dog1 and Dog2 expression. This was further supported by the ability of Dog2 overexpression to restore the growth of *hac1*Δ or *ire1*Δ cells at various concentrations of 2DG (**Fig. 2I**).

2DG also activates the MAPK-based cell-wall integrity pathway which additionally contributes to Dog1 and Dog2 expression

To address a possible additional contribution of other signaling pathways that would contribute to the 2DG-induced expression of Dog1 and Dog2, we ran a bioinformatics analysis on the proteins that were more abundant upon 2DG treatment (**Fig. 1A** and **Data File S1**) using YEASTRACT (*54*) to evaluate whether the observed variations in protein expression could reveal a potential transcriptional signature. The best hit (corresponding to 35/78 candidates, *p*-value=0) was the MADS-box transcription factor Rlm1, a downstream target of the cell wall integrity (CWI) signaling pathway (*55*). The CWI pathway is activated by several stresses such as cell wall damage, and involves plasma membrane-localized sensors, the GTPase Rho1 and its cofactors (guanine nucleotide exchange factors [GEFs] and accessory proteins), protein kinase C, and a cascade leading to the activation of the MAPK Slt2 and downstream transcription factors, such as Rlm1 (**Fig. 3A**) (*55*). There are well-established links between CWI signaling and ER stress (*56-60*); in particular, the CWI pathway is required for viability upon tunicamycin-induced ER stress. Moreover, 2DG causes cell wall defects (*43, 61-63*) and as such might trigger CWI pathway activation. We found that the deletion of many genes in the CWI pathway that act upstream of Rlm1, such as those encoding the sensors *MID2* and *WSC1*, caused an increase in 2DG sensitivity (**Fig. 3B**). Thus, much like the UPR pathway, the CWI pathway is required for 2DG tolerance. 2DG treatment induced the phosphorylation of the MAPK Slt2 within the first hour of exposure (**fig. S4A**). 2DG also triggered the induction of a reporter consisting of an Rlm1-regulated promoter fused to LacZ (**fig. S4B**). Thus, the CWI pathway is activated by 2DG treatment.

We thus questioned whether CWI activation by 2DG contributed to Dog1 and Dog2 induction. Indeed, the activity of both promoters was decreased in the *slt2*Δ mutant (**Fig. 3C** and **S4C**), which was confirmed for Dog2 by analyzing the expression levels of Dog2-GFP (**Fig. 3D-E**). Thus, similarly to tunicamycin (*58*), 2DG induces cell-wall integrity signaling and promotes increased Dog1 and Dog2 expression, in addition to inducing the UPR pathway. These effects may in turn contribute to 2DG tolerance. However, the addition of exogenous mannose did not improve tolerance of CWI mutants to 2DG (**Fig. 3F**). Thus, ER stress relief is not sufficient to suppress 2DG toxicity in these mutants, suggesting that 2DG has other cellular effects beyond triggering ER stress.

A third pathway inhibits the expression of Dog2, but not Dog1, by glucose availability and participates in the resistance of glucose-repression mutants to 2DG

2DG inhibits the activity of hexokinase and phosphoglucose isomerase (*6-8*), thereby impairing glycolysis and leading to energetic stress. Accordingly, 2DG treatment activates AMPK in mammals (*64*). Several lines of evidence indicate that the activity of the yeast AMPK orthologue Snf1 is important for 2DG tolerance. Whereas the *snf1*Δ mutant is hypersensitive to 2DG, the *reg1*Δ mutant, in which Snf1 is hyperactive, displays increased 2DG resistance that depends on Snf1 activity (*31*). We questioned whether some of the resistance or sensitivity phenotypes associated with this pathway (**Fig. 4A**) could be due to an altered level of Dog1 or Dog2 expression, particularly because Snf1 promotes Dog2 expression (*48*). To confirm the effect of Snf1 on Dog1 and Dog2 expression, glucose-grown cells were transferred to a medium containing lactate as a sole carbon source, which should trigger Snf1 activation and consequently, the de-repression of glucose-repressed genes (*65*) (**Fig. 4A**). As expected, switching cells to lactate medium induced Snf1 activation, as determined using antibodies directed against the activated (phosphorylated) form of human AMPKα, which cross-reacts with yeast Snf1 (*66*) (**Fig. 4B**). The expression of Dog2, but not that of Dog1, was increased under these conditions in a Snf1-dependent manner (**Fig. 4B**). In line with these data, the *pDOG2*-LacZ reporter was induced in cells transferred to lactate medium, but this response was decreased in the *snf1Δ* mutant, suggesting that *DOG2* is repressed by glucose and is thus constantly repressed in the *snf1Δ* mutant (**Fig. 4C**), which may explain why the *snf1*Δ mutant is sensitive to 2DG. Although Dog1/2 overexpression in a *snf1Δ* mutant has been reported to not rescue resistance to 2DG (*47*), we thought that this might be because the authors used a high-copy plasmid in which Dog2 expression was still under the control of its endogenous, Snf1-regulated promoter. Indeed, when overexpressed using a strong and constitutive promoter (*pGPD*), Dog2 rescued Snf1 growth in 2DG-exposed cells (**Fig. 4D**).

In contrast, Dog2 expression was increased in glucose-repression mutants which display increased Snf1 activity, such as mutants lacking the hexokinase Hxk2 or the PP1 regulatory phosphatase Reg1

(*44, 67*), both at the promoter and the protein levels (**Fig. 4E-F**). In addition, lack of the Snf1-regulated transcriptional repressors Mig1/Mig2 (**Fig. 4A**) also led to an increase in Dog2 expression (**Fig. 4E-F**). A regulatory sequence in the promoter that is present between -250 and -350 bp relative to the ATG start codon, combined with a proposed Mig1-binding site located at ~200 bp (*40, 48*), was critical for this glucose-mediated repression (**fig. S5, A and B**). The *reg1Δ* or *hxk2Δ* mutants, which are more tolerant to 2DG than WT (*30, 31*), showed increased Dog2 expression (Fig. 4E-F), which was also the case for the double mutant *mig1Δ mig2Δ* (**Fig. 4G**). We deleted *DOG1* and *DOG2* in these mutants to evaluate their contribution to 2DG resistance. The absence of Dog1 and Dog2 sensitized all strains to 2DG (**Fig. 4G**); in particular, the *mig1Δ mig2Δ dog1Δ dog2Δ* showed a level of sensitivity that was comparable to that of the WT, demonstrating that the resistance of the *mig1Δ mig2Δ* mutant was due to increased *DOG* expression. In contrast, the *reg1Δ dog1Δ dog2Δ* and the *hxk2Δ dog1Δ dog2Δ* strains remained more resistant to 2DG than the WT, suggesting additional mechanisms of resistance. Finally, we observed that the *snf1Δ mig1Δ mig2Δ* mutant was resistant to 2DG despite the absence of Snf1, in line with the idea that *snf1Δ* is 2DG-sensitive because of the constitutive repression of Mig1/Mig2 target genes, such as Dog2 and possibly other genes (**Fig. 4F**). Overall, we conclude that Dog2 is also regulated by glucose availability through Snf1 activity, which contributes to the resistance of glucose-repression mutants to 2DG.

Increased expression of *DOG2* is frequently observed in spontaneous 2DG-resistant clones

Previous screens have identified 2DG-resistant mutants (*26, 29, 35*). The initial purpose of these screens was to identify mutants that were insensitive to the repressive effect of 2DG, or that were impaired for glucose phosphorylation (because only 2DG6P is toxic to cells), and consequently, were performed on media containing other carbon sources than glucose. The mechanisms involved in 2DG resistance on glucose medium were tackled later by screening of the deletion library (*30*), which led to the identification of resistant mutants, some of which were subsequently confirmed (*31*). In the course of our experiments, we often found that 2DG-resistant clones could spontaneously arise from

WT or even 2DG-susceptible strains (**Fig. 1E**). Yeast acquires 2DG resistance at a high frequency, which can be accompanied by an increase in 2DG-6-phosphatase activity (*28, 38*). To study whether Dog2, which is functionally critical for 2DG resistance, was upregulated during the emergence of spontaneous 2DG-resistant mutants, we spread ~$2x10^6$ cells on glucose-based medium containing 0.2% 2DG and selected clones that had appeared after 6 days of growth. In total, 24 clones were obtained whose resistance to 2DG was confirmed (**fig. S6A**). Using the p*DOG2*-LacZ reporter, we found that 13 clones displayed significantly increased *DOG2* promoter activity as compared to WT strains (**Fig. 5A**), suggesting that Dog2 overexpression is a frequent feature of 2DG-resistant clones. Among those, we expected to isolate *reg1* and *hxk2* mutants because both are resistant to 2DG in glucose medium (See Figure 5G; *30, 31*). To identify them, we first tested whether some of the isolated resistant clones displayed phenotypes typical of *reg1* mutants, such as sensitivity to tunicamycin (*68, 69*) or selenite (which enters the cell through the glucose-repressed transporter Jen1: *70, 71*). Indeed, three of the isolated clones displayed these phenotypes (**fig. S6A**). Sequencing of the *REG1* coding sequence in these clones revealed the presence of nonsense mutations which likely explain Reg1 loss of function (**fig. S6B**). To identify potential *hxk2* mutants, we performed a complementation test by crossing the 2DG-resistant clones with either a WT strain or an *hxk2Δ* strain and tested the ability of the resulting diploids to grow on 2DG. All diploids generated by the cross with the WT starin lost their ability to grow on 2DG, except for two (clones #23 and #24) (**fig. S6C**), indicating that 2DG resistance was generally caused by a recessive mutation(s). In contrast, 12 diploids obtained by the cross with the *hxk2Δ* strain maintained their ability to grow on 2DG (**fig. S6C**), suggesting that 2DG resistance of the initial strains was caused by a deficiency in *HXK2* function. Sequencing of the *HXK2* ORF in these 12 mutants (**fig. S6D**) revealed that two did not display any mutation in the *HXK2* ORF (clones #1 and #8) and may represent regulatory mutants in *cis*, possibly in regions that were not sequenced. In favor of this hypothesis, we found that their 2DG sensitivity was restored by re-expression of *HXK2* using a multicopy, genomic clone (**fig. S6E**). The other 10 mutants carried at least one mutation in the *HXK2* coding sequence (**fig. S6D**). Four mutants acquired nonsense mutations (clones #12, #15, #16 and #20),

5 mutants (#2, #3, #11, #13 and #14) carried a missense mutation in residues conserved across all hexokinase sequences tested (**fig. S7**, alignment) and one mutant (#21) bore two missense mutations. All of these missense mutations occurred in residues involved in glucose or ATP binding or were located near such residues (**fig. S7**) (*72-74*).

Of the 2DG-resistant clones which expressed *pDOG2*-LacZ at a high level, 2 clones (#9 and #10) lacked mutations in either *REG1* or *HXK2*, suggesting that their resistance involved a mechanism that did not involve these proteins. Whole genome resequencing of the genomic DNA isolated from these clones and comparison with that of the parent strain revealed several SNPs (**Table S1**) including a nonsense mutation in *CYC8* (C^{958}>T) that was identified in both strains, causing a premature stop codon at position 320 (**Fig. 5B**). The *CYC8* gene is also known as *SSN6* (*Suppressor of snf1*) and mutations in this gene lead to constitutive expression of the glucose-repressed gene encoding invertase (*SUC2*), even in a *snf1* mutant (*75, 76*). Indeed, *CYC8* encodes a transcriptional co-repressor which controls the expression of glucose-regulated genes (*77*). Because the repression of *DOG2* expression by glucose is controlled by Snf1 and Mig1/Mig2 (**Fig. 4, E and F**), we hypothesized that *CYC8* could also take part in *DOG2* regulation, such that a mutation in *CYC8* could lead to increased 2DG resistance through *DOG2* overexpression. We observed that indeed, mutants #9 and #10 expressed invertase even in when grown in glucose medium (repressive conditions), in agreement with a mutation in *CYC8* (**Fig. 5C**). We also observed that these mutants displayed increased adhesion, or persistence of colony structures upon washing the plate (*78*) that is often associated with mutants that are prone to flocculation, such as *cyc8* mutants (*79, 80*) (**Fig. 5D**). Introduction of a low copy (centromeric) plasmid containing *CYC8* under the control of its endogenous promoter suppressed the 2DG resistance of mutants #9 and #10 as well as their adhesion to agar plates (**Fig. 5D**). This was not the case when mutants #9 and #10 expressed a truncated version of *CYC8* identified in this screen (**Fig. 5D**), although these mutants did not display slow growth in contrast to the *cyc8Δ* mutant, suggesting that it is at least partially active for other functions. Finally, we tested whether the strong activity of the *DOG2* promoter observed in mutants #9 and #10 (**Fig. 5A**) was also due to the lack of a functional *CYC8*. Indeed, the re-introduction

of low-copy vector containing *CYC8* led to a decreased reporter expression in these mutants (**Fig. 5E**). This result was confirmed by examining Dog2-GFP expression at the protein level (**Fig. 5F-G**). Therefore, *DOG2* expression is repressed by Cyc8 and spontaneous *cyc8* mutants display an increased Dog2 expression. The increased resistance of these mutants to 2DG also depended on the expression of Dog1 and Dog2 as the deletion of *DOG1* and *DOG2* restored their sensitivity to 2DG (**Fig. 5H**). Together, this initial characterization revealed that *DOG2* overexpression is a common phenomenon within spontaneous 2DG-resistant clones, both in known 2DG-resistant mutants (*reg1* and *hxk2*) and in the 2DG-resistant *cyc8* mutants that we isolated.

HDHD1, a human member of the HAD-like phosphatase family, is a 2DG-6-P phosphatase involved in 2DG resistance

The increase in Dog2 expression in various spontaneously 2DG-resistant mutants reminded us of an earlier study in HeLa cells showing increased 2DG6P phosphatase activity in isolated 2DG resistant clones (*20*). Dog1 and Dog2 belong to the family of HAD (haloacid dehalogenase)-like phosphatases which are conserved from bacteria to human (**Fig. 6A**). The bacterial homolog of Dog1/Dog2, named YniC, can also dephosphorylate 2DG6P in vitro (*81*) and we found that the expression of YniC in the double *dog1*Δ *dog2*Δ yeast mutant also restored 2DG resistance (**Fig. 6B**). We used this phenotype to identify potential human homologs (**Fig. 6B**). A PSI-BLAST analysis (*82*) on the human proteome using the Dog2 protein sequence retrieved HDHD1-isoform a (NP_036212.3) as the candidate with highest (39%) homology. HDHD1 (for Haloacid Dehalogenase-like Hydrolase Domain containing 1; also named PUDP for pseudouridine-5'-phosphatase) is a HAD-like phosphatase with in vitro activity towards phosphorylated metabolites such as pseudouridine-5'-phosphate (*83*). When expressed in in the double *dog1*Δ *dog2*Δ mutant, HDHD1 partially rescued growth on 2DG containing medium (**Fig. 6B**). Yeast growth on 2DG was not restored by the expression of HDHD4 (also named NANP, for N-acylneuraminate-9-phosphatase; *84*), which belongs to the same subfamily as HDHD1 within the HAD-phosphatase family (37% homology), or of PSPH (phosphoserine phosphatase; *85*), another close

family member (fig. S8A,B). Moreover, among the four predicted isoforms of HDHD1 (isoforms 1-4), only HDHD1-1 rescued the growth of the *dog1*Δ *dog2*Δ on 2DG-containing medium (fig. S8C) although all isoforms were expressed in yeast, as confirmed by Western blotting using HDHD1 antibodies (fig. S8D).

The mutation of conserved aspartate residues (Asp^{12} and Asp^{14}; Fig. 6A) predicted to be essential for the catalytic activity of HAD phosphatases (*86*) abolished the ability of HDHD1 to restore growth of the *dog1*Δ *dog2*Δ mutant on 2DG (Fig. 6C and fig. S8E), suggesting it may act as a 2DG-6P phosphatase. This notion was confirmed by the ability of purified recombinant HDHD1 (Fig. 6D) to dephosphorylate 2DG-6P in vitro, an activity that required its putative catalytic residues (Fig. 6E). We then tested whether HDHD1 overexpression in HeLa cells could lead to an increased resistance to 2DG. Low concentrations of 2DG (5 mM) in the presence of glucose (25 mM) were sufficient to inhibit the growth of HeLa cells transfected with an empty vector, whereas those that overexpressed HDHD1 were insensitive to 2DG treatment (Fig. 6F). These results suggest that dysregulated expression of HDHD1 could modulate 2DG resistance in human cells.

Discussion

Although the first studies examining the effect of 2DG on glycolysis in yeast and in normal and cancer tissues were published more than 60 years ago (*87-89*), the mode of action for 2DG is not fully understood. 2DG can be considered to be a general competitor of glucose (*90*) and a glycolysis inhibitor because of its inhibition of glycolytic enzymes (*6-8*). However, this view has been challenged because exposure of cancer cells to 2DG interferes with N-linked glycosylation, likely because of the structural similarity of 2DG with mannose (*91*), resulting in ER stress and UPR induction in mammalian cells (*14, 16*). Therefore, 2DG interferes with other cellular functions beyond glycolysis.

In this study, we used an unbiased mass spectrometry approach to analyze the effects of 2DG on the total cellular proteome. We found that the abundance of many glycolytic enzymes was increased, likely because of impaired glycolysis, as well as many genes regulated by the MAPK-based cell wall integrity pathway, suggestive of its activation. Using the list of 2DG-upregulated proteins, we also identified the phosphatases Dog1 and/or Dog2, which have been shown to play a role in 2DG resistance (*33, 40, 41*). Dog2 induction upon 2DG treatment was intriguing because it was not clear how a synthetic molecule such as 2DG could trigger a resistance mechanism. It should be noted that the cellular functions of Dog1 and Dog2, beyond 2DG dephosphorylation, are unknown. They can dephosphorylate various phosphorylated sugars in vitro (*40*), in agreement with the ability of other members of the HAD family of phosphatases to accommodate various substrates (*81*). Therefore, it seemed plausible that Dog1/2 induction was a response to one or more of the cellular consequences of 2DG treatment, rather than to 2DG itself. Our study revealed that the expression of Dog1 and Dog2 was actually controlled by multiple signaling pathways, each of which are activated as a response to 2DG (**Fig. 7**).

This study also probed the signaling pathways that are activated upon 2DG exposure and determined the causes for these activations. First, we confirmed that 2DG triggered ER stress and the onset of the UPR pathway. This finding was not unexpected given the proposed mode of action of this drug and the available data in the literature on mammalian cells (*14, 16*), but had not been formally

proven in yeast with current tools. The induction of an UPR reporter upon 2DG treatment and the hypersensitivity of UPR mutant strains such as *hac1*Δ or *ire1*Δ support this conclusion. The latter phenotype was alleviated by restoring N-glycosylation through the addition of mannose to the culture medium. The consolidation of the links between 2DG and ER stress, notably the identification of UPR mutants as 2DG-hypersensitive mutants suggests that drugs targeting the UPR may synergize with 2DG in a glycolytic cancer background. We also showed that Dog1 and Dog2 are induced by ER stress, in line with high-throughput studies suggesting that Dog1 and Dog2 are UPR-induced genes (*92*).

Second, we showed that 2DG activates the MAPK-based CWI pathway, which mediates the cellular response to cell wall alteration and other stresses. Several studies reported connections between ER stress signaling and the CWI pathway (*56-60*), and 2DG-elicited N-glycosylation defects and ER stress may have repercussions on the CWI pathway. For instance, CWI pathway mutants are sensitive to tunicamycin because they lack an ER surveillance-pathway which normally prevents the inheritance of stressed ER to the daughter cell during cell division (*58*). Many CWI mutants were indeed sensitive to low concentrations (0.05%) of 2DG but unlike UPR mutants, their growth was not restored by the addition of exogenous mannose, suggesting that an N-glycosylation defect is not the sole reason why CWI mutants are hypersensitive to 2DG. However, 2DG interferes with the synthesis of structural polysaccharides that make up the yeast cell wall because 2DG acts as an antagonist of mannose and glucose incorporation into these polymers (*42, 61-63*). 2DG exposure leads to yeast cell lysis at sites of growth, which is where glucan synthesis occurs (*43*) and where the major glucan synthase, Fks1, is localized (*93*). 2DG-induced weakening of the cell wall could trigger the CWI pathway (**Fig. 7**), which would explain why the main sensors responsible for sensing cell wall damage, Wsc1 and Mid2 (reviewed in *55*), are required for growth on 2DG. In addition, we report that the expression of Dog1 and Dog2 was decreased in CWI mutants, which could further sensitize these strains to 2DG. The effect of 2DG on cell wall synthesis suggests an interference of 2DG with UDP-glucose metabolism that is likely to be conserved in metazoans (*94*), where it may affect metabolic pathways involving these precursors, such as glycogen synthesis (*95, 96*).

Our data also revealed that Dog2 expression was regulated at the transcriptional level by glucose availability through the glucose-repression pathway, which is controlled by the kinase Snf1 and the regulatory subunit of the PP1 phosphatase, Reg1. These findings explain why *reg1* mutants have increased 2DG6P phosphatase activity (*28, 38, 39*), because the glucose-mediated repression of Dog2 is defective in these mutants. The negative regulation of Dog2 by this pathway may also contribute to the 2DG resistance of *hxk2* and *mig1* mutants, which participate in the glucose-repression pathways and have been identified in previous screens (*29, 35*). Indeed, the 2DG resistance displayed by the *reg1Δ* and *hxk2Δ* strains partially depended on increased expression of Dog2, because even when these mutants lacked both *DOG* genes, they still grew better than a WT strain on 2DG-containing media. In the *hxk2Δ* mutant, the lack of hexokinase 2 is compensated for by the expression of other glucose-phosphorylating enzymes (such as Hxk1 and the yeast glucokinase homolog, Glk1) (*97*) which may be less prone to phosphorylate 2DG (*36*), and thus could lead to a lower accumulation of 2DG6P in the cell. Hxk2 also has non-metabolic roles beyond sugar phosphorylation (reviewed in Ref. *98*), and loss of these non-metabolic roles may additionally contribute to this phenotype. However, many of the *hxk2* point mutants isolated during the characterization of spontaneous 2DG-resistant clones were affected at or near glucose-binding residues, suggesting a primary metabolic role for Hxk2 in 2DG resistance. Concerning the *reg1*Δ strain, additional mechanisms of resistance beyond an increased expression of Dog2 also remain to be investigated. Previous work suggested that the resistance of the *reg1Δ* mutant depends on Snf1 hyperactivity, because the additional deletion of *SNF1* in this background restores 2DG sensitivity to the *reg1Δ* strain (*31*). Thus, additional Snf1-dependent mechanisms cooperate with the increased expression of *DOG2* to allow *reg1Δ* cells to resist 2DG.

After 2DG import and phosphorylation, the amount of 2DG6P in cells has been reported to exceed that of G6P by up to 80-fold (*99*), although this number should probably be confirmed by more direct and modern methods. Overexpression of Dog2 can revert the repressive effect of 2DG (*33*), suggesting that it can clear the 2DG6P pool up to a point at which 2DG6P is no longer detected by a yet unknown cellular glucose-sensing mechanism. Thus, Dog2 overexpression appears to be a good strategy for

acquiring 2DG resistance, and indeed, Dog2 was overexpressed in the majority of the spontaneously resistant mutants we isolated, including strains with mutations in *REG1* and *HXK2*. Additionally, we identified two mutants carrying a point mutation in the gene encoding the transcriptional repressor Cyc8, leading to a truncated protein at codon 320, within its 8th predicted tetratricopeptide (TPR) repeat. The TPR repeats are involved in the interaction of Cyc8 with its co-repressor Tup1 and in its recruitment to specific promoters, possibly through pathway-specific DNA-binding proteins (*100*). Point mutations in TPR units 9 and 10 affect Cyc8 function in a similar manner as the mutation we isolated (namely, an effect on glucose repression but not global growth), suggesting that alterations at this region only affect a subset of Cyc8 functions (*101*). This finding confirms the differential requirement of TPR repeats for the various functions of Cyc8, and in particular the involvement of the TPR repeats 8-10 in glucose repression (*102*). Together, these data describe *DOG2* overexpression as a successful strategy to overcome 2DG toxicity.

Based on sequence similarity, we identified HDHD1 as an enzyme displaying in vitro 2DG6P phosphatase activity and whose overexpression in both yeast and HeLa cells allowed resistance to 2DG. Whether HDHD1 is responsible for the 2DG resistance previously reported in human cells (*20*) remains to be investigated.

Together, our work shows that 2DG-induced activation of multiple signaling pathways can rewire the expression of endogenous proteins that target 2DG6P to promote 2DG tolerance, and whose increased expression can lead to 2DG resistance. Because of the existence of endogenous genes that can confer 2DG resistance when overexpressed, such as *HDHD1,* and of the perturbation of several cellular pathways in mammalian cells by 2DG, it is possible that similar resistance strategies occur in human cells. Such strategies likely superimpose on other resistance mechanisms that should be scrutinized in the future.

Material and Methods

Yeast strain construction and growth conditions

All yeast strains used in this study derive from the *Saccharomyces cerevisiae* BY4741 or BY4742 background and are listed in **Table S2**. Apart from the mutant strains obtained from the yeast deletion collection (Euroscarf) and the fluorescent GFP tagged strains originating from the yeast GFP clone collection (*103*), all yeast strains were constructed by transformation with the standard lithium acetate-polyethylene glycol protocol using homologous recombination and verified by PCR on genomic DNA prepared with a lithium acetate (200mM) / SDS (0.1%) method (*104*).

Yeast cells were grown in YPD medium (Yeast extract-Peptone-Dextrose 2%) or in synthetic complete medium (SC, containing 1.7g/L yeast nitrogen base (MP Biomedicals), 5g/L ammonium sulfate (Sigma-Aldrich), the appropriate drop-out amino acid preparations (MP Biomedicals) and 2% (w/vol) glucose unless otherwise indicated). Alternatively, SC medium could contain 0.5% lactate as a carbon source (from a 5% stock adjusted to pH=5; Sigma Aldrich). Pre-cultures of 4mL were incubated at 30°C for 8 hours and diluted in fresh medium on the evening to 20mL cultures grown overnight with inoculation optical densities (OD_{600}) of 0.0003 for YPD and 0.001 for SC medium, giving a culture at mid-log phase the next morning.

For glucose depletion experiments, cultures were centrifuged and resuspended in an equal volume of SC/lactate medium and incubated at 30°C during the indicated times. For 2DG, NaCl and tunicamycin treatments, the compounds were added to mid-log phase yeast cultures grown overnight to respective final concentrations of 0.2% (w/v), 400mM and 1µg/mL and incubated for the indicated times. 2-deoxyglucose and tunicamycin were purchased from Sigma-Aldrich. The mannose-supplemented medium (Fig. 2A) consisted of an SC medium that contained all the elements indicated above plus 2% (w/vol) mannose.

Plasmid construction

All the plasmids presented in this study are listed in **Table S3** and were directly constructed in yeast using plasmid homologous recombination (*105*). DNA inserts were amplified by PCR using 70-mer primers containing 50nt homology overhangs and Thermo Fisher Phusion High-fidelity DNA Polymerase and receiver plasmids were digested with restriction enzymes targeting the insertion region. Competent yeast cells rinsed with lithium acetate were incubated for 30 minutes at 30°C with 20µL of the PCR product and 1µL of the plasmid digestion product, followed by a heat shock at 42°C for 20 minutes and a recovery phase in rich medium (YPD) for 90 minutes at 30°C and plated on synthetic medium without uracil. The pDOG1/2-LacZ vectors were generated using the pJEN1-LacZ vector obtained from Bernard Guiard (*106*) and cloning the pDOG1 or pDOG2 promoters (1kb) at *Bgl*II and *Eco*RI sites. The *DOG1*, *DOG2*, *HDHD1* (all four isoforms), *HDHD4*, *PSPH* and *yniC* overexpression

vectors were obtained by digesting a pRS426 vector (2µ, *URA3*) containing the p*GPD* (glyceraldehyde-3-phosphate dehydrogenase gene, *TDH3*) (*107*) promoter with *Eco*RI and *Bam*HI enzymes. In parallel, inserts were PCR-amplified using the following DNA templates: *DOG1* and *DOG2* from yeast genomic DNA preparations (primers: oSL1166/1167 and oSL1141/1142), the *yniC* ORF from *Escherichia coli* DH5α cells (oSL1172/1173) and the human gene ORFs (Uniprot identifiers: HDHD1=Q08623-1/2/3/4, HDHD4=Q8TBE9 and PSPH=P78330) from DNA sequences generated by gene synthesis after codon optimization for yeast expression (Eurofins Genomics) (*HDHD1*: oSL1170/1171 for all isoforms except isoform 3: oSL1170/1216; *HDHD4*: oSL1214/1215; *PSPH*: oSL1212/1213). These PCR products were designed to include a 50-bp overlap with the digested plasmid to enable their cloning by homologous recombination in yeast after co-transformation. The p*GPD-HDHD1*-DDAA vector was obtained by PCR amplification (oSL1155/1171) of the *HDHD1* DNA sequence obtained by gene synthesis using a specific 5' primer carrying two D>A mutations and insertion of this insert into the pRS426 vector digested with EcoRI and BamHI as described above. This construct was verified by sequencing. The DDAA mutant was PCR amplified (oSL1297/oSL1298) and subcloned at NdeI/BamHI sites into pET15b-6His-HDHD1, a kind gift of Dr. E. Van Schaftingen. The wild-type *CYC8* gene and the mutant allele present in mutant #9 were obtained by PCR amplification on the corresponding genomic DNAs with primers (oSL1369/1370) containing a 50-bp overlap with a pRS415 vector (CEN, *LEU2*). The resulting PCR products were digested with XbaI and BamHI, and co-transformed for cloning by homologous recombination in yeast as described above. The plasmids generated in yeast were rescued by extraction (lithium acetate/SDS method (*104*)) and electroporation in bacteria, then amplified and sequenced before being re-transformed in the appropriate strains.

Mass spectrometry and proteomics analyses

Samples used for the proteome-wide analysis of 2-deoxyglucose treatments were prepared from six liquid cultures (WT strain, BY4741) growing overnight at 30°C in 100mL of rich medium with 2% glucose to mid-log phase. On the next morning, 2-deoxyglucose was added to three of the cultures to a final concentration of 0.2% in order to obtain triplicates treated with 2DG and triplicates without drug treatment (negative control). After 2.5 hours of incubation at 30°C, the six cultures were centrifuged at 4000*g* for 5 minutes at 4°C, resuspended in 500*µ*L of 10% trichloroacetic acid (TCA, Sigma-Aldrich) and lysed by shaking after addition of glass beads (0.4-0.6mm, Sartorius) for 10 minutes at 4°C. Cell lysates were retrieved by piercing under the 1.5mL tubes and brief centrifugation. Precipitated proteins were centrifuged at 16000*g* for 10 minutes at 4°C, supernatants were discarded and pellets were rinsed 4 times in 1mL of 100% cold acetone.

Proteins were then digested overnight at 37°C in 20 µL of 25 mM NH_4HCO_3 containing sequencing-grade trypsin (12.5 µg/mL; Promega). The resulting peptides were sequentially extracted with 70% acetonitrile, 0.1% formic acid. Digested samples were acidified with 0.1% formic acid. All digests were

analyzed by an Orbitrap Fusion equipped with an EASY-Spray nanoelectrospray ion source and coupled to an Easy nano-LC Proxeon 1000 system (all from Thermo Fisher Scientific, San Jose, CA). Chromatographic separation of peptides was performed with the following parameters: Acclaim PepMap100 C18 pre-column (2 cm, 75 µm i.d., 3 µm, 100 Å), Pepmap-RSLC Proxeon C18 column (50 cm, 75 µm i.d., 2 µm, 100 Å), 300 nl/min flow, using a gradient rising from 95 % solvent A (water, 0.1 % formic acid) to 40 % B (80 % acetonitrile, 0.1% formic acid) in 120 minutes, followed by a column regeneration of 20 min, for a total run of 140 min. Peptides were analyzed in the orbitrap in full-ion scan mode at a resolution of 120,000 (at *m/z* 200) and with a mass range of *m/z* 350-1550, and an AGC target of $2x10^5$. Fragments were obtained by higher-energy C-trap dissociation (HCD) activation with a collisional energy of 30 %, and a quadrupole isolation window of 1.6 Da. MS/MS data were acquired in the linear ion trap in a data-dependent mode, in top-speed mode with a total cycle of 3 seconds, with a dynamic exclusion of 50 seconds and an exclusion duration of 60 seconds. The maximum ion accumulation times were set to 250 ms for MS acquisition and 30 ms for MS/MS acquisition in parallelization mode.

Raw mass spectrometry data from the Thermo Fisher Orbitrap Fusion were analyzed using the MaxQuant software (*108*) version 1.5.0.7, which includes the Andromeda peptide search engine (*109*). Theoretical peptides were created using the *Saccharomyces cerevisiae* S288C proteome database obtained from Uniprot. Identified spectra were matched to peptides with a main search peptide tolerance of 6ppm. After filtering of contaminants and reverse identifications, the total amount of yeast proteins identified among the six samples was equal to 3425. Protein quantifications were performed using MaxLFQ (*110*) on proteins identified with a minimum amount of two peptides with a False Discovery Rate threshold of 0.05. LFQ values were then analyzed using Perseus (version 1.5.0.15). For the statistical analysis of yeast proteomes treated with 2-dexogylucose compared to negative control samples, each group of triplicates was gathered into a statistical group in order to perform a Student's t-test. Results are presented in the form of Volcano-plots (*111*) and significantly up-regulated and down-regulated candidates were determined by setting an FDR of 0.01 and an S_0 of 2.

GO-term analyses of proteomics data

The 79 significantly up-regulated candidates obtained in the proteomics analysis were used as input for the FunSpec web interface (http://funspec.med.utoronto.ca/) with default settings and a p-value cutoff of 0.01 in order to determine the Gene Ontology biological processes that are enriched in this list of 79 genes compared to the total *Saccharomyces cerevisiae* genome annotation (number of total categories=2062). The complete list of enriched GO biological processes with a p-value<0.01, as well as the genes included in each category, are displayed in Fig. 1B.

Protein extracts and immunoblotting

Yeast cultures used for protein extracts were all grown in synthetic complete medium. For each protein sample, 1.4mL of culture was incubated with 100µL of 100% TCA for 10 minutes on ice to precipitate proteins, centrifuged at 16000*g* at 4°C for 10 minutes and broken for 10 minutes with glass beads, as described for LC-MS/MS sample preparation. Lysates were transferred to another 1.5mL tube and centrifuged 5 minutes at 16000*g* at 4°C, supernatants were discarded and protein pellets were resuspended in 50µL*(OD_{600} of the culture) of sample buffer (50 mM Tris-HCl pH6.8, 100 mM DTT, 2% SDS, 0.1% bromophenol blue, 10% glycerol, complemented with 50mM Tris-Base pH8.8). Protein samples were heated at 95°C for 5 minutes and 10µL were loaded on SDS-PAGE gels (4-20%Mini-PROTEAN TGX Stain-Free, BioRad). After electrophoresis, gels were blotted on nitrocellulose membranes for 60 minutes with a liquid transfer system (BioRad), membranes were blocked in 2% milk for 20 minutes and incubated for at least two hours with the corresponding primary antibodies. Primary and secondary antibodies used in this study as well as their dilutions are listed in **Table S4**. Membranes were washed three times for 10 minutes in Tris-Borate-SDS-Tween20 0.5% buffer and incubated for at least an hour with the corresponding secondary antibody (coupled with Horse Radish Peroxidase). Luminescence signals were acquired with the LAS-4000 imaging system (Fujifilm). Rsp5 was used as a loading control; alternatively, total proteins were visualized in gels using a trihalo compound incorporated in SDS–PAGE gels (stain-free TGX gels, 4–20%; Bio-Rad) after 1 min UV-induced photoactivation and imaging using a Gel Doc EZ Imager (Bio-Rad).

β-galactosidase assays

β-Galactosidase assays were performed using 1mL of mid-log phase yeast cultures carrying the p_{DOG1}-*LacZ* or p_{DOG2}-*LacZ* plasmids, grown overnight in SC medium without uracil with glucose 2% and switched to the specified conditions. The OD (600 nm) of the culture was measured, and samples were taken and centrifuged at 16000*g* at 4°C for 10 minutes. Cell pellets were snap frozen in liquid nitrogen and resuspended in 800µL of Buffer Z (pH=7, 50mM NaH_2PO_4, 45mM Na_2HPO_4, 10mM $MgSO_4$, 10mM KCl and 38mM β-mercaptoethanol). After addition of 160µL of 4mg/mL ONPG (ortho-nitrophenyl-β-D-galactopyranoside, Sigma-Aldrich), samples were incubated at 37°C. Enzymatic reactions were stopped in the linear phase (60min incubation for p_{DOG2}-*LacZ* and 120min incubation for the p_{DOG1}-*LacZ* plasmid, as per initial tests) by addition of 400µL of Na_2CO_3, and cell debris were discarded by centrifugation at 16000*g*. The absorbance of clarified samples was measured with a spectrophotometer set at 420nm. β-Galactosidase activities (arbitrary units, AU) were calculated using the formula $1000*[A_{420}/(A_{600}* t)]$, where A_{420} refers to the enzyme activity and A600 is the turbidity of the culture, and t the incubation time. Each enzymatic assay was repeated independently at least three times.

Drop tests

Yeast cells grown in liquid rich or synthetic complete medium for at least 6 hours at 30°C were adjusted to an optical density (600nm) of 0.5. Serial 10-fold dilutions were prepared in 96-well plates and, using a pin replicator, drops were spotted on plates containing rich or SC medium containing 2% (w/v) agar and when indicated, 2DG (0.05%, or 0.2%, w/vol), sodium selenite (200µM) or tunicamycin (1µg/mL). Mannose plates (Fig 2I and 3F) were prepared as regular SC plates containing 2% mannose (w/vol) in addition to glucose. Plates were incubated at 30°C for 3 to 4 days before scanning. For the adhesion test (Fig. 5D), the plates were scanned and the colonies were then washed with tap water under a constant flow of water for 1 min as previously described (*78*). Excess water was removed before the plates were scanned again.

Isolation of spontaneous mutants and characterization.

WT cells transformed with a p*DOG2*-LacZ plasmid (pSL410) were grown overnight in SC-Ura medium and ca. 2x10(6) cells were spread on SC-Ura plates containing 0.2% 2DG and grown for 6 days at 30°C. The clones obtained (24 clones) were restreaked on SC-Ura to isolate single clones. Resistance to 2DG was confirmed by drop tests (**Fig. S6A**). β-galactosidase enzyme assays and total protein extracts were performed on cultures grown to the exponential phase. For β-galactosidase assays, the results were statistically tested using an unpaired t-test with equal variance, assuming a normal distribution of the values.

Diploids were obtained by crossing each resistant mutant with a WT or *hxk2Δ* strain of the opposite mating type (BY4742, Matα) and selecting single diploid clones on selective medium (SC-Met-Lys). Sequencing of the *REG1* and *HXK2* loci were done after PCR amplification on genomic DNA isolated from the corresponding clones. For whole genome sequencing, genomic DNA of the WT, clone 9 and clone 10 was purified using the Qiagen genomic DNA kit (Genomic-tip 20/G) using 30 OD equivalents of material following the manufacturer's instructions after zymolyase treatment (Seikagaku). A PCR-free library was generated from 10 µg of gDNA and sequenced at the Beijing Genomics Institute (Hong Kong) on Illumina HiSeq 4000. The mutations in each clone were identified through comparative analysis of the variants detected by mapping their reads to the reference genome (BY4741) (*112, 113*) and those detected by mapping the WT reads to the reference. The differential variants were filtered by quality (vcf QUAL>1000) and manually inspected through IGV for validation (*114*).

Cell culture and transfection.

HeLa cells were maintained at 37°C and 5% CO_2 in a humidified incubator and grown in Dulbecco's modified Eagle's medium (DMEM), supplemented with 10% fetal calf serum. Cells were regularly split using Trypsin-EDTA to maintain exponential growth. HeLa cells were transfected with plasmid pCMV-

Sport6-HDHD1 and pCS2 (empty control) using Lipofectamine 2000 according to the manufacturer's instructions. All culture media reagents were from Thermo Fisher Scientific. 2DG (Sigma) was used at a final concentration of 5 mM and tunicamycin (from *Streptomyces sp;* Sigma) was used at a final concentration of 5 µg/mL. For 2DG resistance assays, cells were grown in 10 cm2 flask and split in a 24-well plate in the absence or presence of 5 mM 2DG. Cells were counted each day with a hemocytometer after trypsinization and labeling with Trypan Blue. Total extracts were prepared by incubating cells (10 cm2) on ice for 20 min with 400 µL TSE Triton buffer (50 mM Tris- HCl pH 8.0, NaCl 150 mM, 0.5 mM EDTA, 1% Triton X-100) containing protease inhibitors (cOmplete protease inhibitor cocktail, EDTA-Free, Roche Diagnostics). Cells were then lysed mechanically with scrapers, and the lysate was centrifuged at 13,000 g, 4°C for 30 min. Proteins were assayed in the supernatant using the Bio-Rad Protein Assay reagent (Bio-Rad) and 40 µg proteins were loaded on SDS-PAGE gels.

Recombinant His-tagged HDHD1 and HDHD1-DDAA protein purifications

E. coli BL21 bacteria were transformed with plasmids allowing the expression of His-tagged HDHD1 or HDHD1-DDAA . A 100mL-preculture was grown overnight in LB+Ampicillin (100 µg/mL), diluted 50-fold into 1L culture. The OD reached 0.7-0.9. IPTG (1 mM) was then added to induce the recombinant protein and cells were further grown at 25°C for 3 hours. Cells were harvested, the pellet was frozen in liquid N_2 and thawed on ice. The pellet was resuspended in 20 mL of lysis buffer (HEPES 25mM pH 6.7, 300mM NaCl, imidazole 15 mM, β-mercaptoethanol 2mM, glycerol 10% v/v and protease inhibitor cocktail [cOmplete protease inhibitor cocktail, EDTA-Free, Roche Diagnostics]). Cells were then sonicated and Triton X-100 was added to a final concentration of 1%. The lysate was centrifuged at 12,000rpm in a SW-32 rotor (Beckman Coulter) for 15min at 4°C, and then the supernatant was further centrifuged at 35 000 rpm for 1h at 4°C. The supernatant was incubated with 800 µL of Ni-NTA bead slurry (Qiagen) and rotated overnight at 4°C. The beads were collected by centrifugation (1000*g*, 2min, 4°C), resuspended in lysis buffer, and washed with 50 mL of lysis buffer at 4°C, and then washed again with 50 mL thrombin cleavage buffer (Hepes 50 mM, $CaCl_2$ 5 mM, NaCl 100mM, glycerol 10%) at 4°C. The His-tag was removed by cleavage with 16 U of thrombin (Ref 27-0846-01, Sigma) added directly onto the beads for 2h at 25°C. The eluate was then collected and incubated with 500 µL benzamidine-sepharose 6B (GE Healthcare) at room temperature for 30 min to remove thrombin. The supernatant was collected and protein content was assayed by SDS-PAGE and colloidal blue staining (Brilliant Blue G-colloidal, Sigma), and protein concentration was assayed by the Bradford method (Bio-Rad protein assay, Bio-Rad).

Enzyme assays

2DG6P phosphatase assays were performed in 250 µL of reaction containing 1.5mM 2DG6P (#17149, Cayman Chemicals, Ann Arbor, Michigan, USA) in 50 mM HEPES pH 6.7, 10 mM $MgCl_2$ and 10% glycerol

and 30 µg recombinant HDHD1 or HDHD1-DDAA. Samples were incubated at 37°C for various times (0, 5, 10, 15min) and the reaction was stopped by adding 150µL EDTA (0.5M). Then, the 2DG generated was assayed by adding 500µL of glucose assay reagent (GAGO20, Sigma) and further incubating at 37°C for 30min. The reaction was stopped by adding 500µL H_2SO_4 (12N) and the absorbance of the reaction was measured at 540 nm. A slope (A540 over time) was calculated to assess enzyme activity and to make sure that the reaction was in the linear range. The measurements were repeated 3 times.

Statistical analysis

Mean values calculated using a minimum of three independent measurements from three biological replicates and are plotted with error bars representing standard error of the mean (SEM). Statistical significance was determined using a t-test for paired variables assuming a normal distribution of the values, as follows: *: $P \leq 0.05$; **: $P \leq 0.01$; ***: $P \leq 0.001$; ns: $P > 0.05$.

Supplementary Materials

References and Notes

1. G. Kroemer, J. Pouyssegur, Tumor cell metabolism: cancer's Achilles' heel. *Cancer cell* **13**, 472-482 (2008).
2. J. Yun *et al.*, Glucose deprivation contributes to the development of KRAS pathway mutations in tumor cells. *Science* **325**, 1555-1559 (2009).
3. H. Pelicano, D. S. Martin, R. H. Xu, P. Huang, Glycolysis inhibition for anticancer treatment. *Oncogene* **25**, 4633-4646 (2006).
4. L. Galluzzi, O. Kepp, M. G. Vander Heiden, G. Kroemer, Metabolic targets for cancer therapy. *Nature reviews. Drug discovery* **12**, 829-846 (2013).
5. G. S. Karczmar, J. M. Arbeit, B. J. Toy, A. Speder, M. W. Weiner, Selective depletion of tumor ATP by 2-deoxyglucose and insulin, detected by 31P magnetic resonance spectroscopy. *Cancer Res* **52**, 71-76 (1992).
6. W. Chen, M. Gueron, The inhibition of bovine heart hexokinase by 2-deoxy-D-glucose-6-phosphate: characterization by 31P NMR and metabolic implications. *Biochimie* **74**, 867-873 (1992).
7. A. Sols, R. K. Crane, Substrate specificity of brain hexokinase. *J Biol Chem* **210**, 581-595 (1954).
8. A. N. Wick, D. R. Drury, H. I. Nakada, J. B. Wolfe, Localization of the primary metabolic block produced by 2-deoxyglucose. *J Biol Chem* **224**, 963-969 (1957).
9. D. Zhang *et al.*, 2-Deoxy-D-glucose targeting of glucose metabolism in cancer cells as a potential therapy. *Cancer Lett* **355**, 176-183 (2014).
10. M. Stein *et al.*, Targeting tumor metabolism with 2-deoxyglucose in patients with castrate-resistant prostate cancer and advanced malignancies. *Prostate* **70**, 1388-1394 (2010).
11. B. S. Dwarakanath *et al.*, Clinical studies for improving radiotherapy with 2-deoxy-D-glucose: present status and future prospects. *J Cancer Res Ther* **5 Suppl 1**, S21-26 (2009).
12. L. E. Raez *et al.*, A phase I dose-escalation trial of 2-deoxy-D-glucose alone or combined with docetaxel in patients with advanced solid tumors. *Cancer Chemother Pharmacol* **71**, 523-530 (2013).
13. L. Szablewski, Expression of glucose transporters in cancers. *Biochim Biophys Acta* **1835**, 164-169 (2013).
14. M. Kurtoglu *et al.*, Under normoxia, 2-deoxy-D-glucose elicits cell death in select tumor types not by inhibition of glycolysis but by interfering with N-linked glycosylation. *Molecular cancer therapeutics* **6**, 3049-3058 (2007).
15. L. Andresen *et al.*, 2-deoxy D-glucose prevents cell surface expression of NKG2D ligands through inhibition of N-linked glycosylation. *J Immunol* **188**, 1847-1855 (2012).
16. H. Y. Lin *et al.*, The 170-kDa glucose-regulated stress protein is an endoplasmic reticulum protein that binds immunoglobulin. *Mol Biol Cell* **4**, 1109-1119 (1993).
17. H. Xi *et al.*, 2-Deoxy-D-glucose activates autophagy via endoplasmic reticulum stress rather than ATP depletion. *Cancer Chemother Pharmacol* **67**, 899-910 (2011).
18. M. Pietzke, C. Zasada, S. Mudrich, S. Kempa, Decoding the dynamics of cellular metabolism and the action of 3-bromopyruvate and 2-deoxyglucose using pulsed stable isotope-resolved metabolomics. *Cancer Metab* **2**, 9 (2014).
19. S. Kavaliauskiene *et al.*, Novel actions of 2-deoxy-D-glucose: protection against Shiga toxins and changes in cellular lipids. *Biochem J* **470**, 23-37 (2015).

20. S. Barban, Studies on the mechanism of resistance to 2-deoxy-D-glucose in mammalian cell cultures. *J Biol Chem* **237**, 291-295 (1962).
21. R. Diaz-Ruiz, M. Rigoulet, A. Devin, The Warburg and Crabtree effects: On the origin of cancer cell energy metabolism and of yeast glucose repression. *Biochim Biophys Acta* **1807**, 568-576 (2011).
22. J. L. Celenza, M. Carlson, A yeast gene that is essential for release from glucose repression encodes a protein kinase. *Science* **233**, 1175-1180 (1986).
23. J. O. Nehlin, H. Ronne, Yeast MIG1 repressor is related to the mammalian early growth response and Wilms' tumour finger proteins. *EMBO J* **9**, 2891-2898 (1990).
24. L. L. Lutfiyya, M. Johnston, Two zinc-finger-containing repressors are responsible for glucose repression of SUC2 expression. *Mol Cell Biol* **16**, 4790-4797 (1996).
25. M. Conrad *et al.*, Nutrient sensing and signaling in the yeast Saccharomyces cerevisiae. *FEMS Microbiol Rev* **38**, 254-299 (2014).
26. F. K. Zimmermann, I. Scheel, Mutants of Saccharomyces cerevisiae resistant to carbon catabolite repression. *Mol Gen Genet* **154**, 75-82 (1977).
27. R. B. Bailey, A. Woodword, Isolation and characterization of a pleiotropic glucose repression resistant mutant of Saccharomyces cerevisiae. *Mol Gen Genet* **193**, 507-512 (1984).
28. M. F. Heredia, C. F. Heredia, Saccharomyces cerevisiae acquires resistance to 2-deoxyglucose at a very high frequency. *J Bacteriol* **170**, 2870-2872 (1988).
29. L. Neigeborn, M. Carlson, Mutations causing constitutive invertase synthesis in yeast: genetic interactions with snf mutations. *Genetics* **115**, 247-253 (1987).
30. M. Ralser *et al.*, A catabolic block does not sufficiently explain how 2-deoxy-D-glucose inhibits cell growth. *Proc Natl Acad Sci U S A* **105**, 17807-17811 (2008).
31. R. R. McCartney, D. G. Chandrashekarappa, B. B. Zhang, M. C. Schmidt, Genetic analysis of resistance and sensitivity to 2-deoxyglucose in Saccharomyces cerevisiae. *Genetics* **198**, 635-646 (2014).
32. I. Witt, R. Kronau, H. Holzer, Repression von Alkoholdehydrogenase, Malatdehydrogenase, Isocitratlyase und Malatsynthase in Hefe durch Glucose. *Biochim Biophys Acta* **118**, 522-537 (1966).
33. F. Randez-Gil, J. A. Prieto, P. Sanz, The expression of a specific 2-deoxyglucose-6P phosphatase prevents catabolite repression mediated by 2-deoxyglucose in yeast. *Current genetics* **28**, 101-107 (1995).
34. K. Hedbacker, M. Carlson, Regulation of the nucleocytoplasmic distribution of Snf1-Gal83 protein kinase. *Eukaryot Cell* **5**, 1950-1956 (2006).
35. H. J. Schuller, K. D. Entian, Extragenic suppressors of yeast glucose derepression mutants leading to constitutive synthesis of several glucose-repressible enzymes. *J Bacteriol* **173**, 2045-2052 (1991).
36. Z. Lobo, P. K. Maitra, Physiological role of glucose-phosphorylating enzymes in Saccharomyces cerevisiae. *Arch Biochem Biophys* **182**, 639-645 (1977).
37. P. K. Maitra, A glucokinase from Saccharomyces cerevisiae. *J Biol Chem* **245**, 2423-2431 (1970).
38. C. F. Heredia, A. Sols, Metabolic Studies with 2-Deoxyhexoses. II. Resistance to 2-Deoxyglucose in a Yeast Mutant. *Biochim Biophys Acta* **86**, 224-228 (1964).
39. M. Martin, C. F. Heredia, Characterization of a phosphatase specific for 2-deoxyglucose-6-phosphate in a yeast mutant. *FEBS Lett* **83**, 245-248 (1977).

40. F. Randez-Gil, A. Blasco, J. A. Prieto, P. Sanz, DOGR1 and DOGR2: two genes from Saccharomyces cerevisiae that confer 2-deoxyglucose resistance when overexpressed. *Yeast* **11**, 1233-1240 (1995).
41. P. Sanz, F. Randez-Gil, J. A. Prieto, Molecular characterization of a gene that confers 2-deoxyglucose resistance in yeast. *Yeast* **10**, 1195-1202 (1994).
42. C. F. Heredia, G. de la Fuente, A. Sols, Metabolic Studies with 2-Deoxyhexoses. I. Mechanisms of Inhibition of Growth and Fermentation in Baker's Yeast. *Biochim Biophys Acta* **86**, 216-223 (1964).
43. B. F. Johnson, Lysis of yeast cell walls induced by 2-deoxyglucose at their sites of glucan synthesis. *J Bacteriol* **95**, 1169-1172 (1968).
44. R. R. McCartney, M. C. Schmidt, Regulation of Snf1 kinase. Activation requires phosphorylation of threonine 210 by an upstream kinase as well as a distinct step mediated by the Snf4 subunit. *The Journal of biological chemistry* **276**, 36460-36466 (2001).
45. K. Hedbacker, M. Carlson, SNF1/AMPK pathways in yeast. *Front Biosci* **13**, 2408-2420 (2008).
46. J. Tu, M. Carlson, REG1 binds to protein phosphatase type 1 and regulates glucose repression in Saccharomyces cerevisiae. *EMBO J* **14**, 5939-5946 (1995).
47. A. F. O'Donnell *et al.*, 2-Deoxyglucose impairs *Saccharomyces cerevisiae* growth by stimulating Snf1-regulated and alpha-arrestin-mediated trafficking of hexose transporters 1 and 3. *Mol Cell Biol* **35**, 939-955 (2015).
48. Y. Tsujimoto, S. Izawa, Y. Inoue, Cooperative regulation of DOG2, encoding 2-deoxyglucose-6-phosphate phosphatase, by Snf1 kinase and the high-osmolarity glycerol-mitogen-activated protein kinase cascade in stress responses of Saccharomyces cerevisiae. *J Bacteriol* **182**, 5121-5126 (2000).
49. K. Tatebayashi, M. Takekawa, H. Saito, A docking site determining specificity of Pbs2 MAPKK for Ssk2/Ssk22 MAPKKKs in the yeast HOG pathway. *EMBO J* **22**, 3624-3634 (2003).
50. T. Stevens, B. Esmon, R. Schekman, Early stages in the yeast secretory pathway are required for transport of carboxypeptidase Y to the vacuole. *Cell* **30**, 439-448 (1982).
51. Y. Kozutsumi, M. Segal, K. Normington, M. J. Gething, J. Sambrook, The presence of malfolded proteins in the endoplasmic reticulum signals the induction of glucose-regulated proteins. *Nature* **332**, 462-464 (1988).
52. J. S. Cox, P. Walter, A novel mechanism for regulating activity of a transcription factor that controls the unfolded protein response. *Cell* **87**, 391-404 (1996).
53. B. M. Gardner, D. Pincus, K. Gotthardt, C. M. Gallagher, P. Walter, Endoplasmic reticulum stress sensing in the unfolded protein response. *Cold Spring Harb Perspect Biol* **5**, a013169 (2013).
54. M. C. Teixeira *et al.*, The YEASTRACT database: a tool for the analysis of transcription regulatory associations in Saccharomyces cerevisiae. *Nucleic acids research* **34**, D446-451 (2006).
55. D. E. Levin, Regulation of cell wall biogenesis in Saccharomyces cerevisiae: the cell wall integrity signaling pathway. *Genetics* **189**, 1145-1175 (2011).
56. M. Bonilla, K. W. Cunningham, Mitogen-activated protein kinase stimulation of Ca(2+) signaling is required for survival of endoplasmic reticulum stress in yeast. *Mol Biol Cell* **14**, 4296-4305 (2003).

57. S. A. Krause, H. Xu, J. V. Gray, The synthetic genetic network around PKC1 identifies novel modulators and components of protein kinase C signaling in *Saccharomyces cerevisiae*. *Eukaryot Cell* **7**, 1880-1887 (2008).
58. A. Babour, A. A. Bicknell, J. Tourtellotte, M. Niwa, A surveillance pathway monitors the fitness of the endoplasmic reticulum to control its inheritance. *Cell* **142**, 256-269 (2010).
59. Y. Chen *et al.*, Identification of mitogen-activated protein kinase signaling pathways that confer resistance to endoplasmic reticulum stress in Saccharomyces cerevisiae. *Mol Cancer Res* **3**, 669-677 (2005).
60. T. Scrimale, L. Didone, K. L. de Mesy Bentley, D. J. Krysan, The unfolded protein response is induced by the cell wall integrity mitogen-activated protein kinase signaling cascade and is required for cell wall integrity in Saccharomyces cerevisiae. *Mol Biol Cell* **20**, 164-175 (2009).
61. Z. Kratky, P. Biely, S. Bauer, Mechanism of 2-deoxy-D-glucose inhibition of cell-wall polysaccharide and glycoprotein biosyntheses in Saccharomyces cerevisiae. *Eur J Biochem* **54**, 459-467 (1975).
62. R. Datema, R. T. Schwarz, Formation of 2-deoxyglucose-containing lipid-linked oligosaccharides. Interference with glycosylation of glycoproteins. *Eur J Biochem* **90**, 505-516 (1978).
63. P. Biely, Z. Kratky, J. Kovarik, S. Bauer, Effect of 2-deoxyglucose on cell wall formation in Saccharomyces cerevisiae and its relation to cell growth inhibition. *J Bacteriol* **107**, 121-129 (1971).
64. D. B. Shackelford, R. J. Shaw, The LKB1-AMPK pathway: metabolism and growth control in tumour suppression. *Nat Rev Cancer* **9**, 563-575 (2009).
65. H. J. Schuller, Transcriptional control of nonfermentative metabolism in the yeast Saccharomyces cerevisiae. *Current genetics* **43**, 139-160 (2003).
66. M. Orlova, L. Barrett, S. Kuchin, Detection of endogenous Snf1 and its activation state: application to Saccharomyces and Candida species. *Yeast* **25**, 745-754 (2008).
67. M. A. Treitel, S. Kuchin, M. Carlson, Snf1 protein kinase regulates phosphorylation of the Mig1 repressor in Saccharomyces cerevisiae. *Mol Cell Biol* **18**, 6273-6280 (1998).
68. J. Ferrer-Dalmau, F. Randez-Gil, M. Marquina, J. A. Prieto, A. Casamayor, Protein kinase Snf1 is involved in the proper regulation of the unfolded protein response in Saccharomyces cerevisiae. *Biochem J* **468**, 33-47 (2015).
69. T. Mizuno, Y. Masuda, K. Irie, The Saccharomyces cerevisiae AMPK, Snf1, Negatively Regulates the Hog1 MAPK Pathway in ER Stress Response. *PLoS Genet* **11**, e1005491 (2015).
70. M. Becuwe, S. Leon, Integrated control of transporter endocytosis and recycling by the arrestin-related protein Rod1 and the ubiquitin ligase Rsp5. *eLife* **3**, 03307 (2014).
71. J. R. McDermott, B. P. Rosen, Z. Liu, Jen1p: a high affinity selenite transporter in yeast. *Mol Biol Cell* **21**, 3934-3941 (2010).
72. P. Kuser, F. Cupri, L. Bleicher, I. Polikarpov, Crystal structure of yeast hexokinase PI in complex with glucose: A classical "induced fit" example revised. *Proteins* **72**, 731-740 (2008).
73. P. Bork, C. Sander, A. Valencia, An ATPase domain common to prokaryotic cell cycle proteins, sugar kinases, actin, and hsp70 heat shock proteins. *Proc Natl Acad Sci U S A* **89**, 7290-7294 (1992).

74. A. E. Aleshin *et al.*, Crystal structures of mutant monomeric hexokinase I reveal multiple ADP binding sites and conformational changes relevant to allosteric regulation. *J Mol Biol* **296**, 1001-1015 (2000).
75. M. Carlson, B. C. Osmond, L. Neigeborn, D. Botstein, A suppressor of SNF1 mutations causes constitutive high-level invertase synthesis in yeast. *Genetics* **107**, 19-32 (1984).
76. R. J. Trumbly, Isolation of Saccharomyces cerevisiae mutants constitutive for invertase synthesis. *J Bacteriol* **166**, 1123-1127 (1986).
77. L. G. Vallier, M. Carlson, Synergistic release from glucose repression by mig1 and ssn mutations in *Saccharomyces cerevisiae*. *Genetics* **137**, 49-54 (1994).
78. C. G. Guldal, J. Broach, Assay for adhesion and agar invasion in S. cerevisiae. *J Vis Exp*, e64 (2006).
79. R. J. Rothstein, F. Sherman, Genes affecting the expression of cytochrome c in yeast: genetic mapping and genetic interactions. *Genetics* **94**, 871-889 (1980).
80. A. W. Teunissen, J. A. van den Berg, H. Y. Steensma, Transcriptional regulation of flocculation genes in Saccharomyces cerevisiae. *Yeast* **11**, 435-446 (1995).
81. E. Kuznetsova *et al.*, Genome-wide analysis of substrate specificities of the Escherichia coli haloacid dehalogenase-like phosphatase family. *J Biol Chem* **281**, 36149-36161 (2006).
82. S. F. Altschul *et al.*, Gapped BLAST and PSI-BLAST: a new generation of protein database search programs. *Nucleic acids research* **25**, 3389-3402 (1997).
83. A. Preumont, R. Rzem, D. Vertommen, E. Van Schaftingen, HDHD1, which is often deleted in X-linked ichthyosis, encodes a pseudouridine-5'-phosphatase. *Biochem J* **431**, 237-244 (2010).
84. P. Maliekal, D. Vertommen, G. Delpierre, E. Van Schaftingen, Identification of the sequence encoding N-acetylneuraminate-9-phosphate phosphatase. *Glycobiology* **16**, 165-172 (2006).
85. A. Seifried, J. Schultz, A. Gohla, Human HAD phosphatases: structure, mechanism, and roles in health and disease. *FEBS J* **280**, 549-571 (2013).
86. A. M. Burroughs, K. N. Allen, D. Dunaway-Mariano, L. Aravind, Evolutionary genomics of the HAD superfamily: understanding the structural adaptations and catalytic diversity in a superfamily of phosphoesterases and allied enzymes. *J Mol Biol* **361**, 1003-1034 (2006).
87. F. B. Cramer, G. E. Woodward, 2-Desoxy-D-glucose as an antagonist of glucose in yeast fermentation. *Journal of the Franklin Institute* **253**, 354-360 (1952).
88. G. E. Woodward, F. B. Cramer, M. T. Hudson, Carbohydrate analogs as antagonists of glucose in carbohydrate metabolism of yeast. *Journal of the Franklin Institute* **256**, 577-587 (1953).
89. G. E. Woodward, M. T. Hudson, The effect of 2-desoxy-D-glucose on glycolysis and respiration of tumor and normal tissues. *Cancer Res* **14**, 599-605 (1954).
90. G. E. Woodward, 2-desoxy-d-glucose as an inhibitor in the aerobic glucose metabolism of yeast. *Journal of the Franklin Institute* **254**, 553-555 (1952).
91. H. T. Kang, E. S. Hwang, 2-Deoxyglucose: an anticancer and antiviral therapeutic, but not any more a low glucose mimetic. *Life Sci* **78**, 1392-1399 (2006).
92. K. J. Travers *et al.*, Functional and genomic analyses reveal an essential coordination between the unfolded protein response and ER-associated degradation. *Cell* **101**, 249-258 (2000).

93. T. Utsugi *et al.*, Movement of yeast 1,3-beta-glucan synthase is essential for uniform cell wall synthesis. *Genes Cells* **7**, 1-9 (2002).
94. M. F. Schmidt, R. T. Schwarz, C. Scholtissek, Nucleoside-diphosphate derivatives of 2-deoxy-D-glucose in animal cells. *Eur J Biochem* **49**, 237-247 (1974).
95. H. Xi, M. Kurtoglu, T. J. Lampidis, The wonders of 2-deoxy-D-glucose. *IUBMB Life* **66**, 110-121 (2014).
96. P. Biely, V. Farkas, S. Bauer, Incorporation of 2-deoxy-D-glucose into glycogen. *Biochim Biophys Acta* **158**, 487-488 (1968).
97. A. Rodriguez, T. De La Cera, P. Herrero, F. Moreno, The hexokinase 2 protein regulates the expression of the GLK1, HXK1 and HXK2 genes of Saccharomyces cerevisiae. *Biochem J* **355**, 625-631 (2001).
98. J. M. Gancedo, The early steps of glucose signalling in yeast. *FEMS Microbiol Rev* **32**, 673-704 (2008).
99. S. C. Kuo, J. O. Lampen, Inhibition by 2-deoxy-D-glucose of synthesis of glycoprotein enzymes by protoplasts of Saccharomyces: relation to inhibition of sugar uptake and metabolism. *J Bacteriol* **111**, 419-429 (1972).
100. N. Gounalaki, D. Tzamarias, M. Vlassi, Identification of residues in the TPR domain of Ssn6 responsible for interaction with the Tup1 protein. *FEBS Lett* **473**, 37-41 (2000).
101. N. Maqani *et al.*, Spontaneous mutations in CYC8 and MIG1 suppress the short chronological lifespan of budding yeast lacking SNF1/AMPK. *Microb Cell* **5**, 233-248 (2018).
102. D. Tzamarias, K. Struhl, Distinct TPR motifs of Cyc8 are involved in recruiting the Cyc8-Tup1 corepressor complex to differentially regulated promoters. *Genes Dev* **9**, 821-831 (1995).
103. W. K. Huh *et al.*, Global analysis of protein localization in budding yeast. *Nature* **425**, 686-691 (2003).
104. M. Looke, K. Kristjuhan, A. Kristjuhan, Extraction of genomic DNA from yeasts for PCR-based applications. *Biotechniques* **50**, 325-328 (2011).
105. H. Ma, S. Kunes, P. J. Schatz, D. Botstein, Plasmid construction by homologous recombination in yeast. *Gene* **58**, 201-216 (1987).
106. T. Lodi, F. Fontanesi, B. Guiard, Co-ordinate regulation of lactate metabolism genes in yeast: the role of the lactate permease gene JEN1. *Mol Genet Genomics* **266**, 838-847 (2002).
107. D. Mumberg, R. Muller, M. Funk, Yeast vectors for the controlled expression of heterologous proteins in different genetic backgrounds. *Gene* **156**, 119-122 (1995).
108. J. Cox, M. Mann, MaxQuant enables high peptide identification rates, individualized p.p.b.-range mass accuracies and proteome-wide protein quantification. *Nat Biotechnol* **26**, 1367-1372 (2008).
109. J. Cox *et al.*, Andromeda: a peptide search engine integrated into the MaxQuant environment. *Journal of proteome research* **10**, 1794-1805 (2011).
110. J. Cox *et al.*, Accurate proteome-wide label-free quantification by delayed normalization and maximal peptide ratio extraction, termed MaxLFQ. *Mol Cell Proteomics* **13**, 2513-2526 (2014).
111. N. C. Hubner, M. Mann, Extracting gene function from protein-protein interactions using Quantitative BAC InteraCtomics (QUBIC). *Methods* **53**, 453-459 (2011).
112. H. Li, R. Durbin, Fast and accurate short read alignment with Burrows-Wheeler transform. *Bioinformatics* **25**, 1754-1760 (2009).

113. A. McKenna *et al.*, The Genome Analysis Toolkit: a MapReduce framework for analyzing next-generation DNA sequencing data. *Genome Res* **20**, 1297-1303 (2010).
114. J. T. Robinson *et al.*, Integrative genomics viewer. *Nat Biotechnol* **29**, 24-26 (2011).
115. J. A. Vizcaino *et al.*, 2016 update of the PRIDE database and its related tools. *Nucleic acids research* **44**, 11033 (2016).
116. R. B. Trimble, F. Maley, Subunit structure of external invertase from Saccharomyces cerevisiae. *J Biol Chem* **252**, 4409-4412 (1977).

Acknowledgments: We would like to thank Nicolas Joly (Institut Jacques Monod, Paris, France) for discussions about the HDHD1 in vitro assay; Gaelle Lelandais (I2BC, Gif-sur-Yvette, France) for help with the use of Yeastract analysis and advices on statistical analysis; Pascual Sanz (Instituto de Biomedicina de Valencia, Valencia, Spain) and Jose Antonio Prieto (Instituto de Agroquímica y Tecnología de Alimentos, Valencia, Spain) for the gift of the GST-Dog2 construct; Emile Van Schaftingen (de Duve Institute, Université Catholique de Louvain, Louvain-la-Neuve, Belgium) for the gift of the His-tagged HDHD1 construct; Peter Walter (UCSF, San Francisco, CA, USA) for the gift of the *pUPRE1*:lacZ reporter; David Levin (Boston University, Boston, MA, USA) for the gift of the pCYC(2xRlm1):lacZ reporter; Colin Stirling (University of Manchester, Manchester, UK) for the gift of the anti-invertase antibody and Martin Schmidt (University of Pittsburgh, Pittsburgh, PA, USA) for advice regarding gDNA extraction for sequencing. We also thank Thibaut Léger and the Proteomics facility of the Institut Jacques Monod (supported by the Region Ile-de-France (SESAME), the Paris-Diderot University (ARS), and CNRS) for assistance. We thank Anna Babour (IUH, Hôpital Saint Louis, Paris, France), Alenka Čopič (Institut Jacques Monod, Paris, France), Myriam Ruault (Institut Curie, Paris, France), Eric Chevet (CLCC Eugène Marquis, Rennes, France) and members of the Léon and Chevet labs for insightful comments and critical reading. **Funding**: This work was supported by fellowships from the Fondation pour la Recherche Médicale (SPF20150934065 to QD) and the Ligue contre le cancer (TAZK20115 to CL), and by grants from the Agence Nationale de la Recherche (P-Nut, ANR-16-CE13-0002 to SL) and the Fondation ARC pour la recherche sur le cancer (PJA20181208080 to SL). **Author contributions**: QD, AV, CL, SL contributed reagents, performed experiments, and acquired and analyzed the data. AF and JS analyzed the genome sequencing data. SL and QD wrote the manuscript. SL directed the work. **Competing interests:** The authors declare that they have no competing interests. **Data and materials availability**: The mass spectrometry proteomics data have been deposited to the ProteomeXchange Consortium via the PRIDE (*115*) partner repository with the dataset identifier PXD014373. All other data needed to evaluate the conclusions in the paper are present in the paper or the Supplementary Materials.

Figure Legends

Figure 1. Proteomics analysis of the response to 2DG in yeast reveals transcriptional induction of the 2DG6P phosphatases Dog1 and Dog2.

(**A**) Volcano-plot representing changes in protein abundance in total protein extracts of wild-type (WT) yeast in response to 2DG (0.2%), obtained by mass spectrometry-based proteomics and analyzed with MaxQuant software. The x axis corresponds to the $\log_2$ value of the abundance ratio (LFQ: Label-Free Quantification) between 2DG treatment and the negative control. The y axis represents the $-\log_{10}$ of the *p*-value of the statistical t-test for each quantified protein (n=3 independent biological replicates). Lines: threshold with a False Discovery Rate of 0.01. (**B**) Gene Ontology (GO) analysis of the proteins identified as upregulated in response to 2DG treatment along with their *p*-value and the proteins included in each category. (**C**) Western blot on total protein extracts of yeast cells expressing endogenously tagged Dog1-GFP or Dog2-GFP, before and after 2DG addition for the indicated times, using an anti-GFP antibody. A longer exposure is displayed for Dog1-GFP cells to highlight the higher abundance of Dog1 after 2DG addition. Rsp5, whose levels did not change upon 2DG addition in all of our experiments, is used as a loading control. (n=2 independent experiments.) (**D**) β-galactosidase assays of wild-type yeast cells expressing *LacZ* under the control of the p*DOG1* or p*DOG2* promoters, before and after 2DG treatments for 3 hours (± SEM, *n*=3 independent experiments, t-test). (**E**) Serial dilutions of cultures from the indicated strains were spotted onto SD plates containing no DG or 0.05% 2DG and grown for 3 days at 30°C. (n=2 independent experiments.) (**F**) β-galactosidase assays of wild-type and *hog1Δ* strains expressing *LacZ* under the control of the p*DOG2* promoter, before and after 2DG treatments for 3 hours (± SEM, *n*=3 independent experiments, t-test). (**G**) Western blot on total protein extracts of WT and *hog1Δ* cells endogenously expressing a Dog2-GFP fusion, before and after 2DG addition for 3h, using an anti-GFP antibody. Total protein was visualized in gels using a trihalo compound. Glc, glucose. (**H**) Relative expression of Dog2-GFP in the same conditions as (**G**) after normalization to total protein and using WT/untreated as a reference (± SEM, *n*=3 independent experiments, t-test).

Figure 2. 2DG treatment induces Dog2 expression through glycosylation defects that trigger ER stress and the Unfolded Protein Response.

(**A**) WT cells were grown overnight to mid-log phase in SC medium, centrifuged and resuspended in SC-medium containing mannose (2%) or not, and treated with 0.2% 2DG or 1µg/mL tunicamycin (Tm) for 4 hours. Total protein extracts were Western blotted for Carboxypeptidase Y (CPY). (n=3 independent experiments.) Glc, glucose. Glycosyl., glycosylation. (**B**) Schematic of the UPR signaling

pathway in yeast showing how ER stress triggers Ire1-mediated splicing of the pre-mRNA encoding the transcription factor Hac1 and the subsequent induction of UPR target genes. (**C**) β-galactosidase assays on WT and *hac1Δ* cells expressing *LacZ* under the control of an UPR-inducible promoter (p*UPRE1*) and treated with 0.2% 2DG or 1µg/mL tunicamycin for 3 hours (± SEM, *n*=3 independent experiments, t-test). (**D**) β-galactosidase assays on WT cells expressing *LacZ* under the control of the *DOG2* promoter and treated as in (**C**) (± SEM, *n*=3 independent experiments, t-test). (**E**) β-galactosidase assays on WT and *hac1Δ* cells expressing *LacZ* under the control the *DOG2* promoter, before and after 3h 2DG treatments (± SEM, *n*=3 independent experiments, t-test). (**F**) Western blot for GFP on total protein extracts of WT and *hac1Δ* cells endogenously expressing a Dog2-GFP fusion, before and after 3h treatment with 2DG or tunicamycin. (**G**) Relative expression of Dog2-GFP under the same conditions as (**F**) after normalization to total protein and using WT/untreated as a reference (± SEM, *n*=3 independent experiments, t-test). (**H**) Serial dilutions of cultures from the indicated strains were spotted onto SC plates (supplemented with 2% mannose when indicated) containing no DG or 0.05% 2DG, and were grown for 3 days at 30°C. (n=2 independent experiments.) (**I**) Serial dilutions of cultures from the indicated strains overexpressing *DOG2* (*pGPD-DOG2)* or not (Ø) were spotted onto SC-Ura plates containing 0, 0.05% or 0.2% 2DG. The plates were scanned after 3 days of incubation at 30°C. (n=2 independent experiments.)

Figure 3. 2DG activates the MAPK-based CWI pathway, which is required for 2DG tolerance and additionally contributes to the regulation of Dog2 expression.

(**A**) Schematic of the CWI pathway showing the various components and their requirement for growth on 2DG (see color code in the inset) based on drop tests shown in (**B**). (**B**) Serial dilutions of cultures from the indicated deletion strains were spotted onto SD plates containing no DG or 0.05% 2DG and grown for 3 days at 30°C. (n=2 independent experiments.) (**C**) β-galactosidase assays on WT and *slt2Δ* cells expressing *LacZ* under the control the *DOG2* promoter, before and after 3h 2DG treatments (± SEM, *n*=3 independent experiments, t-test). (**D**) Western blot on total protein extracts of WT and *slt2Δ* cells expressing an endogenously tagged Dog2-GFP fusion, before and after 3h treatment with 2DG, using an anti-GFP antibody. (**E**) Relative expression of Dog2-GFP in the same conditions as (**D**) after normalization to total protein and using WT/untreated as a reference (± SEM, *n*=3 independent experiments, t-test). (**F**) Serial dilutions of cultures from the indicated strains were spotted onto SC plates (supplemented with 2% mannose when indicated) containing no DG or 0.05% 2DG and were grown for 3 days at 30°C. (n=2 independent experiments.)

Figure 4. *DOG2*, but not *DOG1*, is negatively controlled by glucose availability through transcriptional repression by Mig1-Mig2 and the kinase Snf1.

(**A**) Schematic of the glucose repression pathway showing how Snf1 (the yeast homolog of AMPK), PP1 (composed of Glc7 and Reg1 subunits) and their downstream transcriptional repressors Mig1/Mig2 regulate glucose-repressed genes in response to glucose availability or absence (such in the presence of lactate). (**B**) WT and *snf1Δ* strains, both expressing endogenously tagged Dog1-TAP and Dog2-GFP fusions, were grown overnight in SC medium and then either treated with 0.2% 2DG or switched to an SC-lactate medium for 4 hours. Dog1-TAP was detected with the peroxidase-anti-peroxidase (PAP) complex and Dog2-GFP with anti-GFP antibodies, phosphorylated (p) Snf1 with anti-phospho-AMPK and total Snf1 with an anti-polyHis tag (because Snf1 contains a stretch of 13 histidine residues that can be used for its detection) (n=2 independent experiments.) (**C**) β-galactosidase activity on WT and *snf1Δ* cells expressing *LacZ* under the control the *DOG1* or the *DOG2* promoter, before and after 3h growth in lactate. The fold-induction after transfer to lactate is indicated for each promoter in each strain (± SEM, *n*=4 independent experiments). (**D**) WT and *snf1Δ* strains, transformed with either a genomic clone containing both *DOG1* and *DOG2* under the control of its own promoter (*pend:DOG*), or with a vector containing *DOG2* under the control of the strong *GPD* promoter (*pGPD:DOG2*) were grown, serial-diluted and spotted onto SC plates (SC-Leu or SC-Ura) with or without 0.2% DG, and grown for 3 days at 30°C. (n=2 independent experiments.) (**E**) β-galactosidase assays on WT and the indicated deletion mutants expressing *LacZ* under the control the *DOG2* promoter after overnight growth in SC medium (exponential phase) (± SEM, *n*=6 independent experiments). (**F**) The indicated strains, all expressing an endogenously tagged Dog2-GFP fusion, were grown overnight in SC medium (to exponential phase). Total protein extracts were immunoblotted with anti-GFP antibodies. Rsp5 was used as a loading control. (n=2 independent experiments.) (**G**) Serial dilutions of cultures of the indicated mutants were spotted on YPD plates containing 0, 0.2% or 0.5% of 2DG. Plates were scanned after 3 days of growth at 30°C. (n=3 independent experiments.)

Figure 5. The characterization of spontaneous 2DG-resistant strains identifies mutants showing increased Dog2 expression, including a new mutant allele of *CYC8*.

(**A**) 24 clones showing a spontaneous resistance to 0.2% 2DG were isolated. The β-galactosidase activity of these mutants, due to the expression of the *LacZ* reporter driven by the *DOG2* promoter, was measured after overnight growth in SC medium (to exponential phase) (± SEM, *n*=4 independent experiments, t-test). Colors represent the identity of the mutants as determined in **fig. S6 A-B** for *reg1* and **fig. S6 C-E** for *hxk2* and **B**-**G** for *cyc8*. (**B**) Schematic of the domain organization of the Cyc8 protein, showing the Poly(Q) and Poly(QA) repeats as well as the N-terminal TPR repeats. Red: mutation identified by whole genome resequencing of the spontaneous 2DG-resistant mutants #9 and #10. (**C**)

A WT strain, the mutant strains #9 and #10 and the *reg1Δ* mutant (used as a positive control) were grown in SC medium (to exponential phase). Total protein extracts were immunoblotted for invertase (invertase is heavily glycosylated and migrates as a smear (*116*)). (n=2 independent experiments.) (**D**) WT and mutants #9 and #10 were transformed with low-copy (centromeric) plasmid either empty or containing WT *CYC8* or mutant *cyc8* (Gln^{320}*), and were spotted on SC-Leu or SC-Leu + 0.2% 2DG medium, and grown for 3 days at 30°C. Middle panel: the control plate was scanned and then washed for 1 min under a constant flow of water, and then scanned again. (n=2 independent experiments.) (**E**) β-galactosidase activity on WT and mutants #9 and #10 expressing *LacZ* under the control the *DOG2* promoter and transformed with an empty vector or a low-copy vector containing WT *CYC8*, after growth in SC medium (normalized to the value of the WT, ± SEM, *n*=3 independent experiments, t-test). (**F**) Western blot on total protein extracts of WT and mutants #9 and #10 cells expressing an endogenously tagged Dog2-GFP fusion and transformed with either an empty plasmid or a low-copy (centromeric) plasmid containing WT *CYC8* after growth in SC medium, using an anti-GFP antibody. (**G**) Relative expression of Dog2-GFP in the same conditions as (**F**) after normalization by total proteins and using the WT control as a reference (± SEM, *n*=3 independent experiments, t-test). (**H**) Serial dilutions of cultures of the indicated mutants were spotted on SC medium or SC + 0.2% 2DG medium and grown for 3 days at 30°C (n=2 independent experiments). mut, mutant.

Figure 6. The human phosphatase HDHD1 has a 2DG6P phosphatase activity and its overexpression leads to 2DG resistance in HeLa cells.

(**A**) Multiple protein sequence alignment of yeast Dog1, Dog2, *Escherichia* coli yniC and the human proteins HDHD1, HDHD4 and PSPH aligned with ClustalX 2.0. The highly conserved catalytic aspartates are displayed in yellow. The six first amino-acids of PSPH were truncated to optimize the N-terminal alignment of its catalytic aspartates with the other phosphatases. (**B**) Serial dilutions of WT and *dog1Δdog2Δ* strains transformed with the indicated plasmids were spotted on SC-Ura medium with or without 0.05% 2DG and were scanned after 3 days of growth at 30°C. (n=2 independent experiments.) (**C**) Serial dilutions of *dog1Δdog2Δ* strains transformed with an empty vector or vectors allowing the expression of a HDHD1 or its predicted catalytic mutant, HDHD1-DD>AA (in which the N-terminal catalytic aspartates were mutated to alanines) were spotted on SC-Ura medium with or without 0.05% 2DG and were scanned after 3 days of growth at 30°C. (n=2 independent experiments.) (**D**) Recombinant, His-tagged HDHD1 and HDHD1-DD>AA were expressed in bacteria and purified for in vitro enzymatic tests. 0.7µg were loaded on a gel to show homogeneity of the protein purification. (**E**) In vitro 2DG6P phosphatase activity of HDHD1 and HDHD1>DDAA as measured by assaying glucose release from 2DG6P. (n=3 independent experiments.) (**F**) Growth of HeLa cells transfected with an empty vector (□) or with a construct allowing the overexpression of HDHD1 (○) over time in the

absence (open symbols) or presence (filled symbol) of 5mM 2DG. The number of cells is normalized to that of the untransformed/untreated cells after 3 days (± SEM, *n*=3 independent experiments, t-test).

Figure 7. Working Model.

Glucose phosphorylation triggers the onset of the glucose-repression pathway in which PP1 inactivates Snf1. This leads to the lack of phosphorylation of Mig1 and Mig2, which remain in the nucleus to mediate the glucose-repression of genes such as *DOG2*. The deletion of *REG1*, *HXK2*, or *MIG1* and *MIG2* or a mutation in *CYC8* leads to 2DG resistance, which is at least partially mediated through increased expression of *DOG2*, leading to the dephosphorylation of 2DG-6-P. In contrast, the deletion of *SNF1* causes an increased sensitivity to 2DG, which can be rescued by the deletion of *MIG1* and *MIG2* or by Dog2 overexpression. In parallel, 2DG6P causes (i) ER stress and triggers the UPR pathway, which stimulates *DOG2* expression through the transcription factor Hac1, and (ii) the CWI pathway, likely through interference with polysaccharide and cell wall synthesis, which also induces *DOG2* through the transcription factor Rlm1.

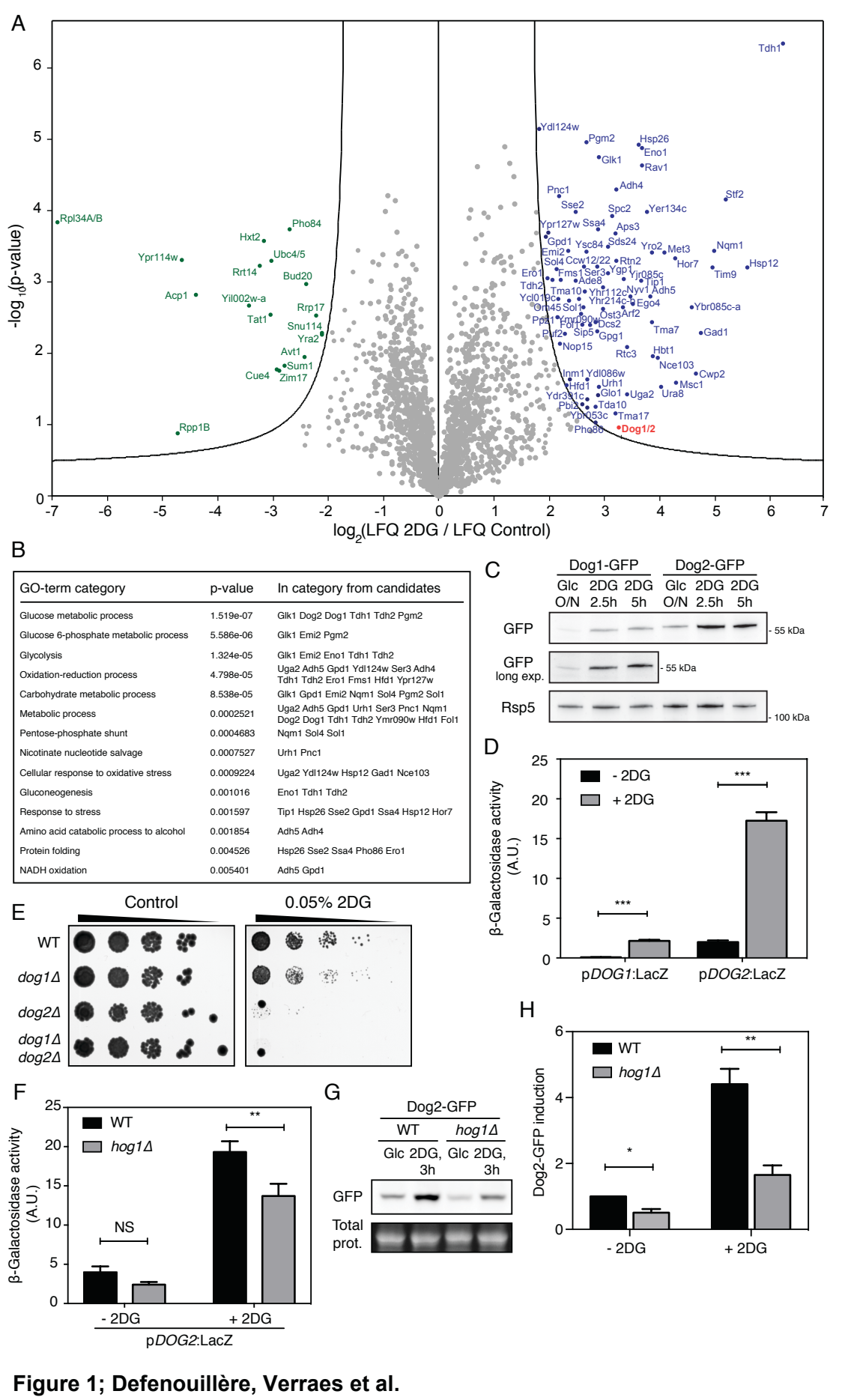

GO-term category	p-value	In category from candidates
Glucose metabolic process	1.519e-07	Glk1 Dog2 Dog1 Tdh1 Tdh2 Pgm2
Glucose 6-phosphate metabolic process	5.586e-06	Glk1 Emi2 Pgm2
Glycolysis	1.324e-05	Glk1 Emi2 Eno1 Tdh1 Tdh2
Oxidation-reduction process	4.798e-05	Uga2 Adh5 Gpd1 Ydl124w Ser3 Adh4 Tdh1 Tdh2 Ero1 Fms1 Hfd1 Ypr127w
Carbohydrate metabolic process	8.538e-05	Glk1 Gpd1 Emi2 Nqm1 Sol4 Pgm2 Sol1
Metabolic process	0.0002521	Uga2 Adh5 Gpd1 Urh1 Ser3 Pnc1 Nqm1 Dog2 Dog1 Tdh1 Tdh2 Ymr090w Hfd1 Fol1
Pentose-phosphate shunt	0.0004683	Nqm1 Sol4 Sol1
Nicotinate nucleotide salvage	0.0007527	Urh1 Pnc1
Cellular response to oxidative stress	0.0009224	Uga2 Ydl124w Hsp12 Gad1 Nce103
Gluconeogenesis	0.001016	Eno1 Tdh1 Tdh2
Response to stress	0.001597	Tip1 Hsp26 Sse2 Gpd1 Ssa4 Hsp12 Hor7
Amino acid catabolic process to alcohol	0.001854	Adh5 Adh4
Protein folding	0.004526	Hsp26 Sse2 Ssa4 Pho86 Ero1
NADH oxidation	0.005401	Adh5 Gpd1

Figure 1; Defenouillère, Verraes et al.

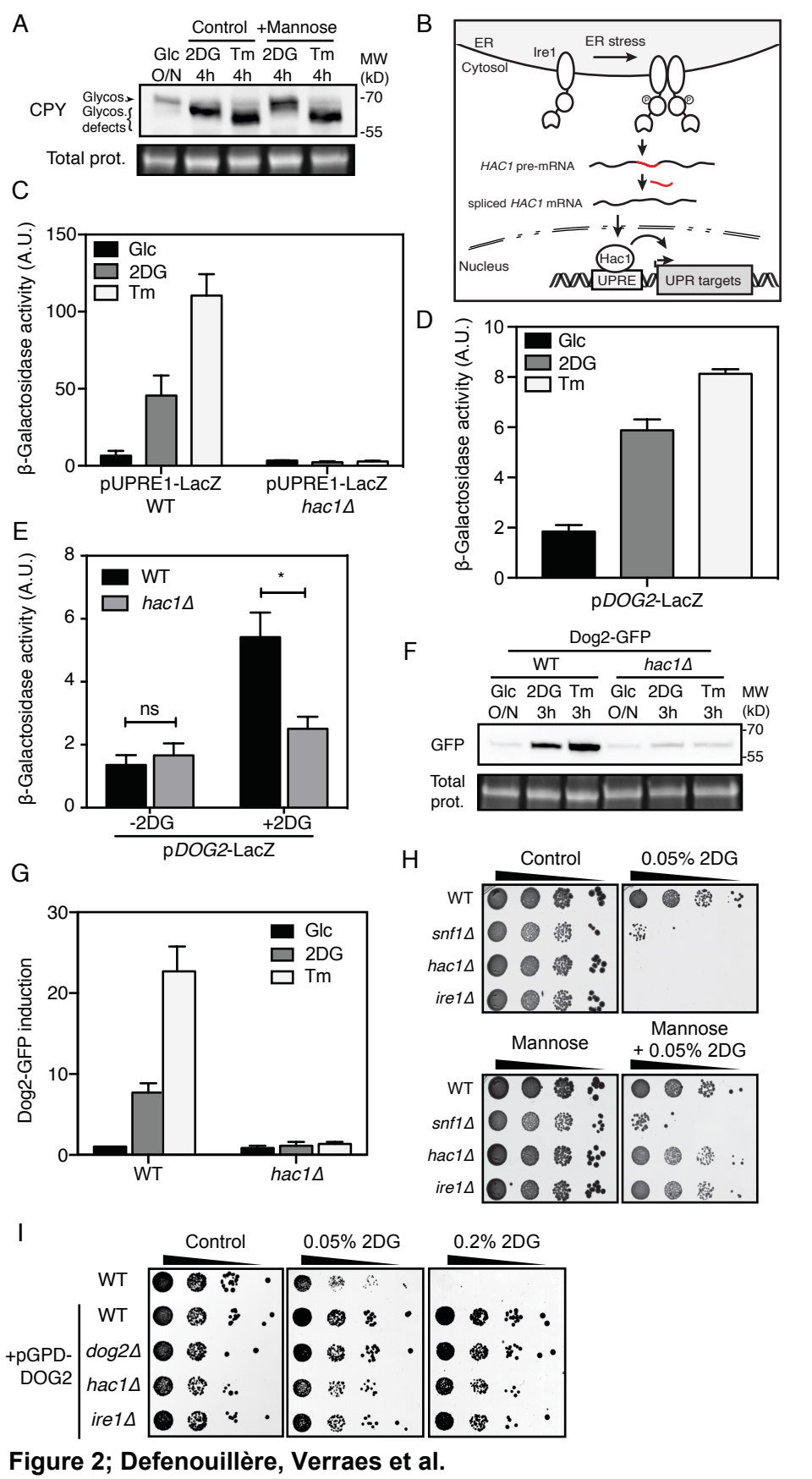

Figure 2; Defenouillère, Verraes et al.

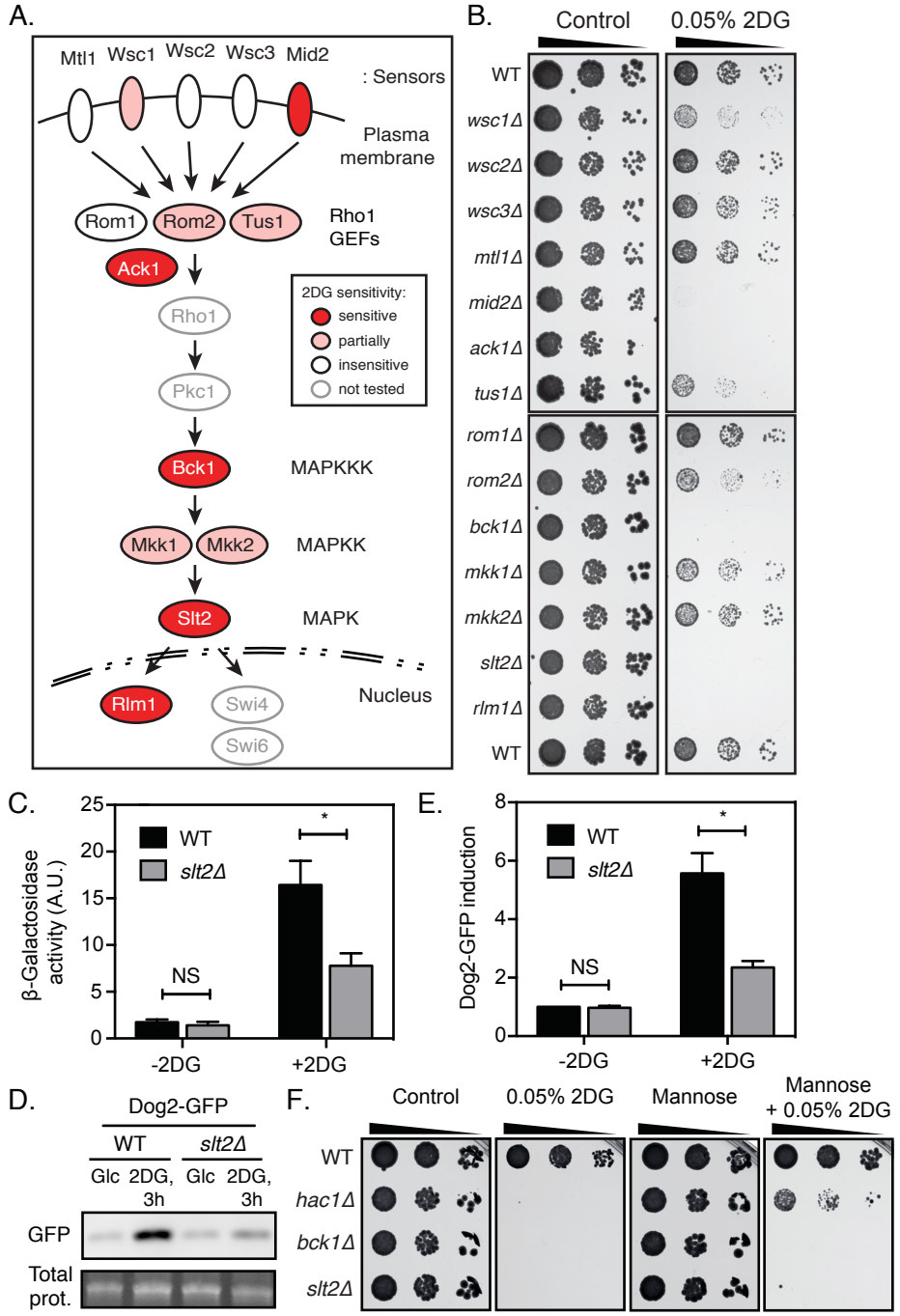

Figure 3; Defenouillère, Verraes et al.

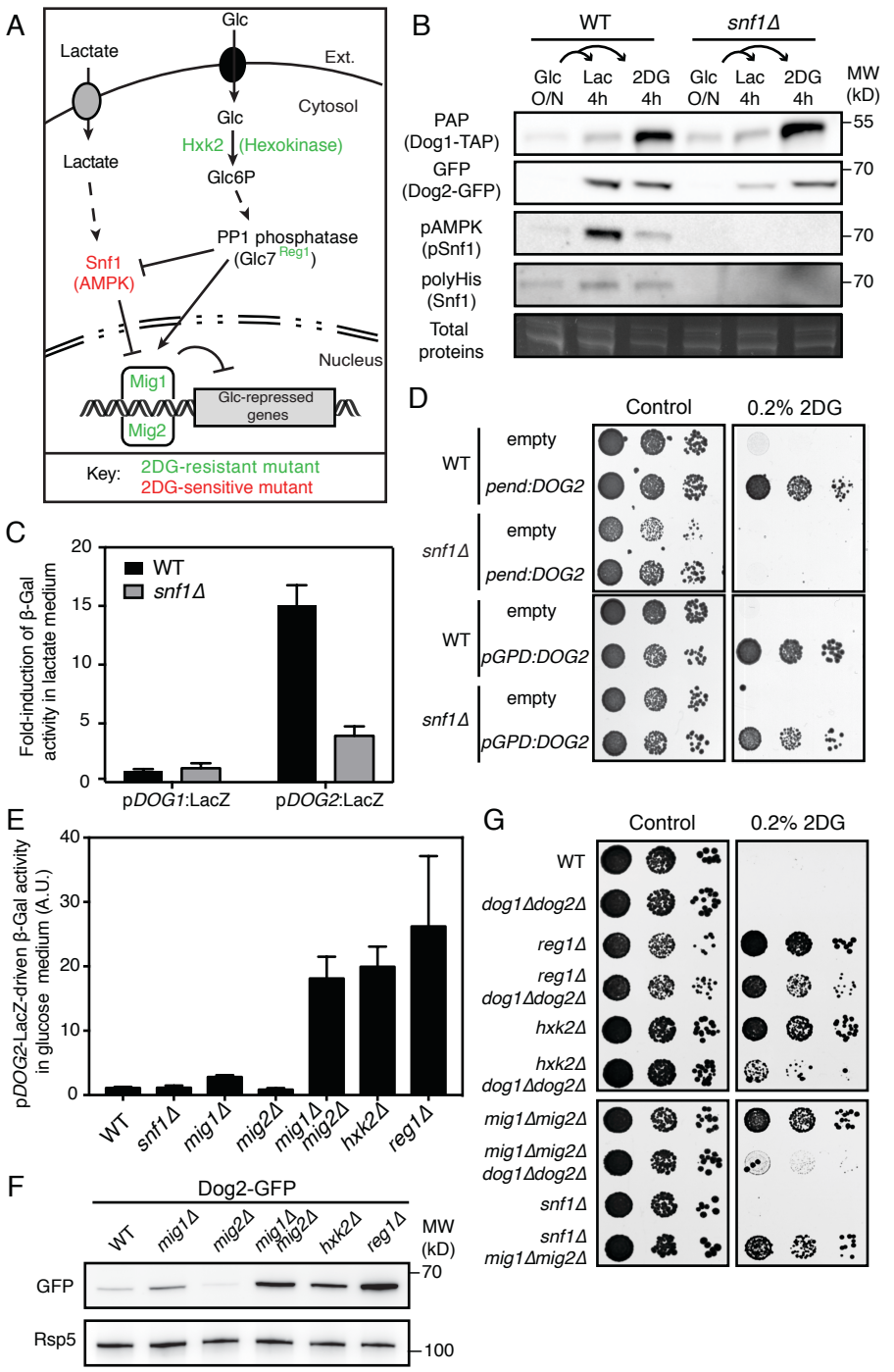

Figure 4; Defenouillère, Verraes et al.

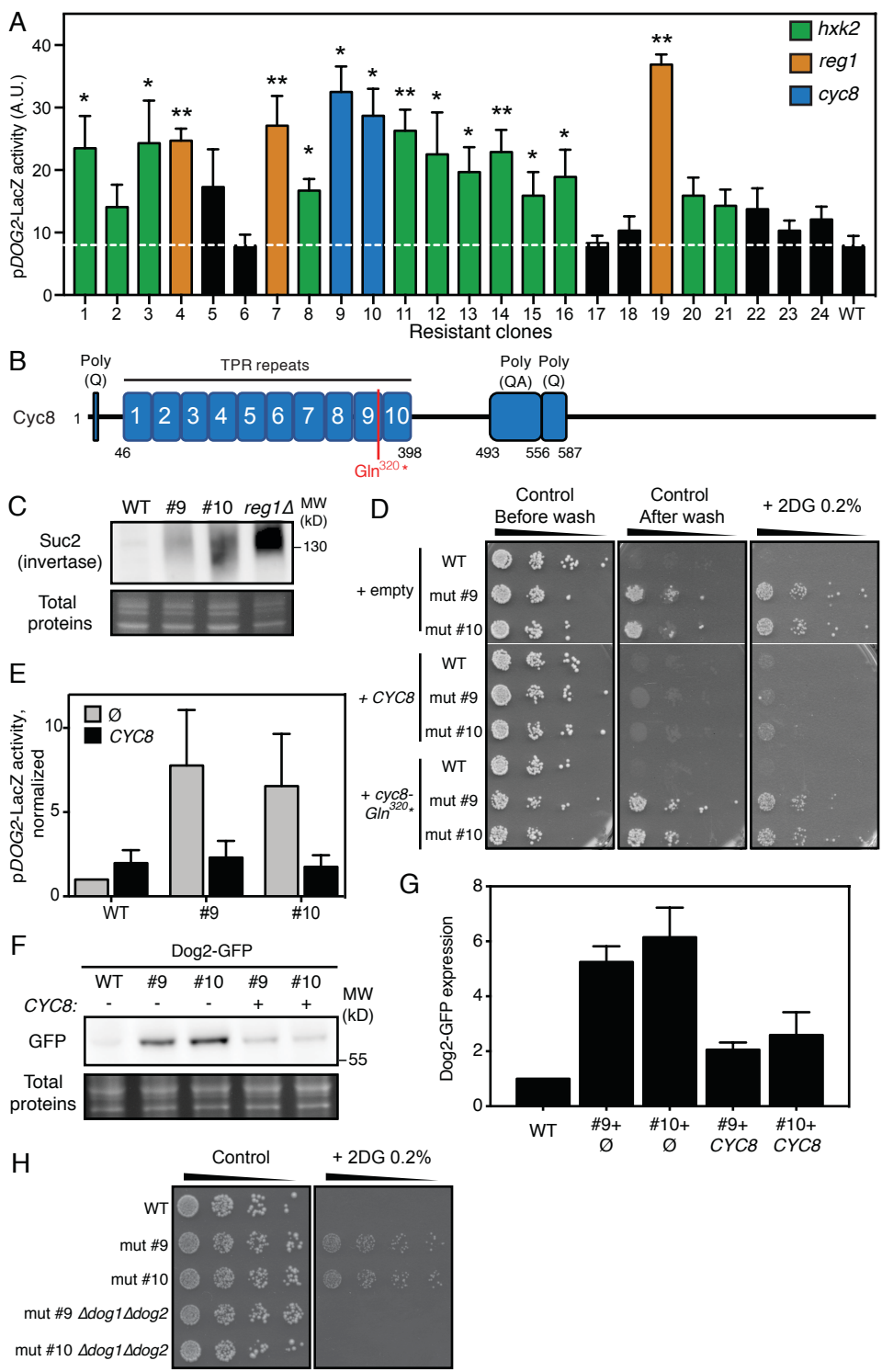

Figure 5; Defenouillère, Verraes et al

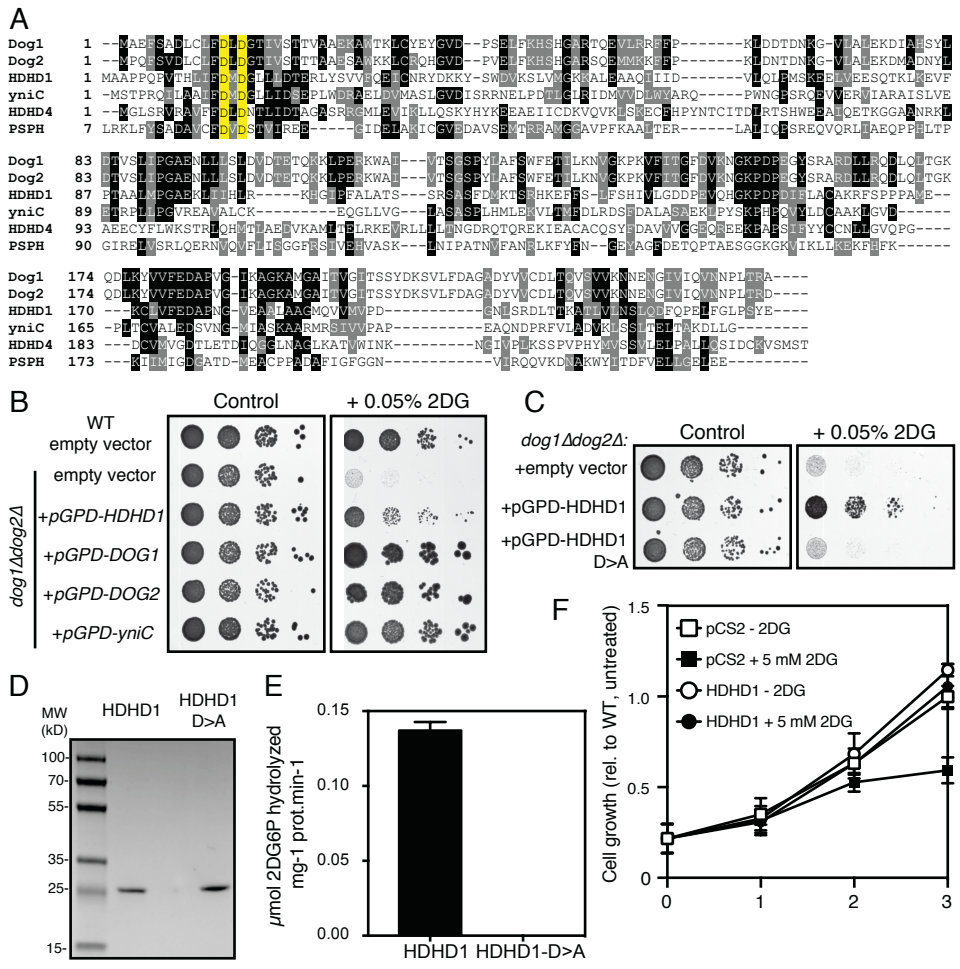

Figure 6; Defenouillère, Verraes et al.

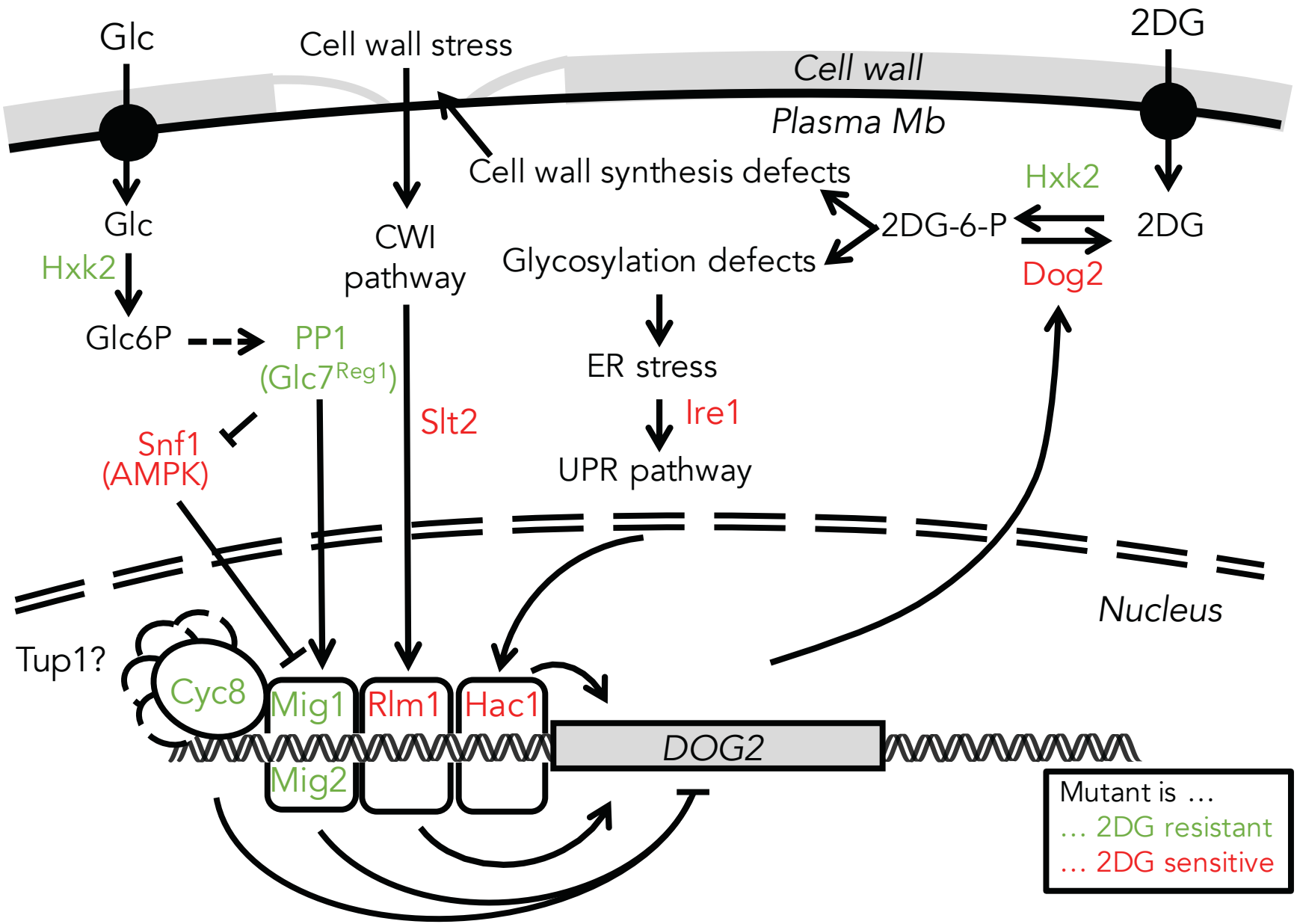

Figure 7; Defenouillère, Verraes et al.

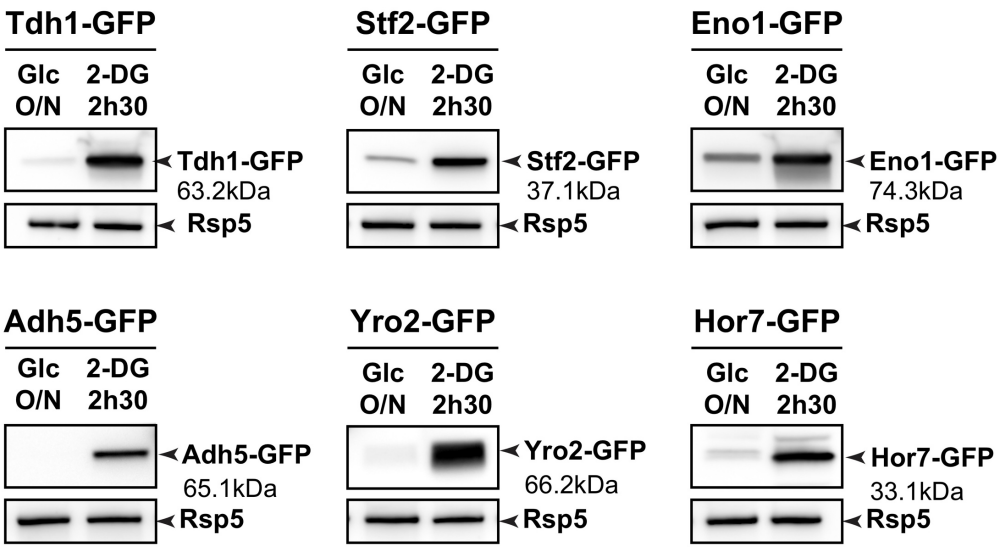

Figure S1. Characterization of other candidates showing increased abundance after 2DG treatment.
Western blot for GFP on total protein extracts of yeast cells expressing the indicated endogenously GFP-tagged proteins, before and after 2.5h 2DG addition. Rsp5 is used as a loading control. (n=3 independent experiments.)

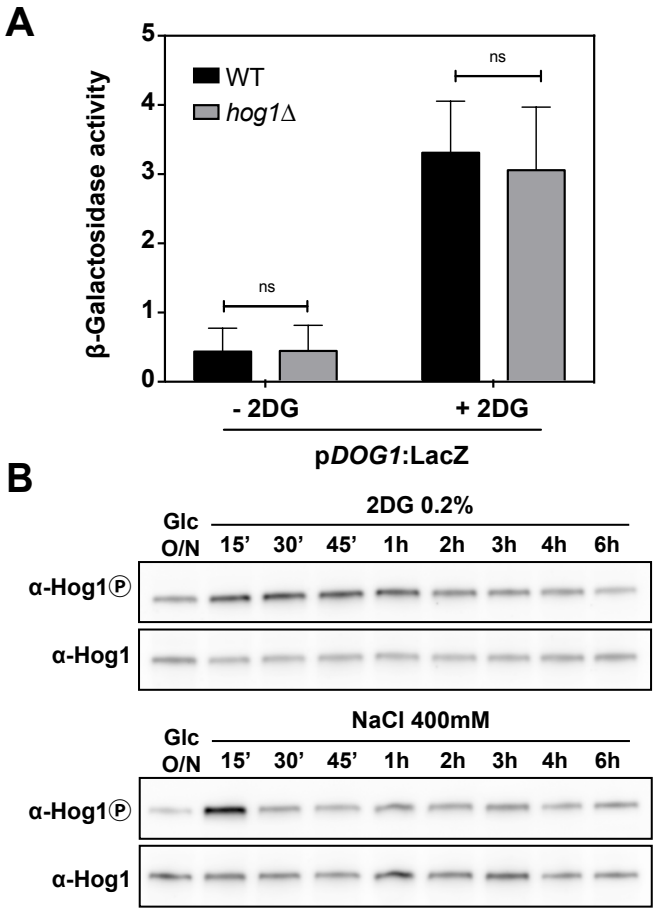

Figure S2. Hog1 signaling responds to 2DG but *DOG1* expression is not regulated by Hog1. (**A**). β-galactosidase assays of wild-type and *hog1*Δ strains expressing *LacZ* under the control of the p*DOG1* promoter, before and after 2DG treatments for 3 hours. Error bars: SEM (*n*=3 independent experiments, t-test). (**B**). Western blot on total extracts of wild-type yeast cells grown overnight in SD medium and treated with 0.2% 2DG or 400mM NaCl for the indicated times. The anti-phospho-p38/Hog1 antibody enables the detection of phosphorylated Hog1 and Hog1 is used as a control for Hog1 abundance throughout the time course. (n=2 independent experiments.)

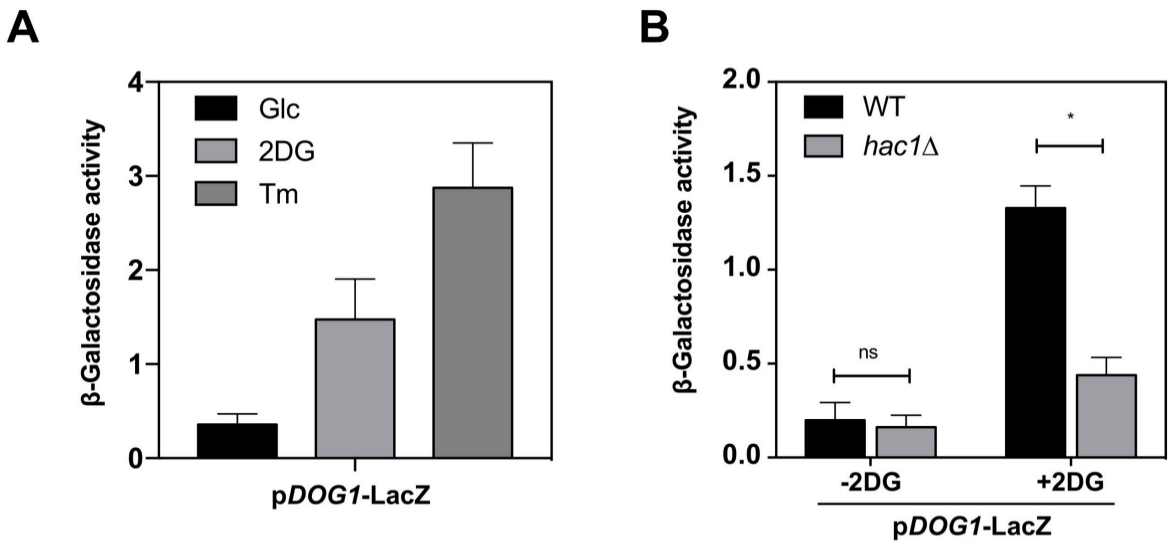

Figure S3. *DOG1* expression is regulated by the UPR pathway.
(**A**). β-galactosidase assays on WT cells expressing *LacZ* under the control of the *DOG1* promoter and treated with 0.2% 2DG or 1µg/mL tunicamycin for 3 hours (± SEM, *n*=3 independent experiments, t-test). (**B**). β-galactosidase assays on WT and *hac1*Δ cells expressing *LacZ* under the control of the *DOG1* promoter, before and after 3h 2DG treatments (± SEM, *n*=4 independent experiments, *: $p<0.05$).

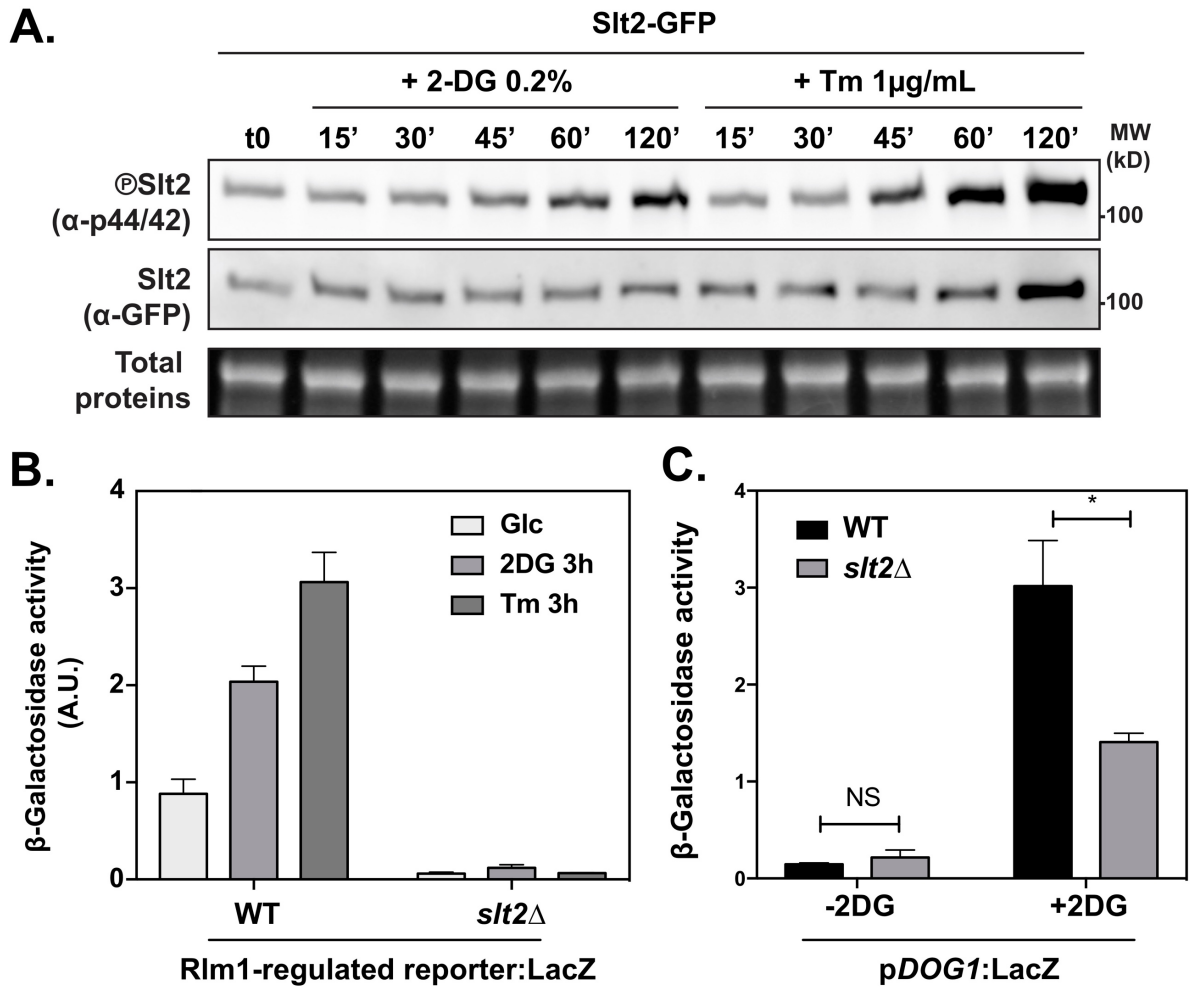

Figure S4. Slt2 participates in the regulation of *DOG1* expression.
(**A**) A WT strain expressing an endogenously-tagged Slt2-GFP construct was grown in SC medium and treated with 2DG (0.2%) or tunicamycin (1 µg/mL). Total protein extracts were prepared at the indicated times and blotted with the following antibodies: anti-p44/42, to reveal activated (phosphorylated) Slt2, and anti-GFP to reveal total levels of Slt2. (n=2 independent experiments.) (**B**) β-galactosidase assays on WT and *slt2*Δ cells expressing *LacZ* under the control of an Rlm1-regulated promoter, before and after 3h 2DG (0.2%) or tunicamycin (1 µg/mL) treatments (± SEM, *n*=3 independent experiments, t-test). (**C**) β-galactosidase assays on WT and *slt2*Δ cells expressing *LacZ* under the control the *DOG1* promoter, before and after 3h 2DG treatments (± SEM, *n*=3 independent experiments, t-test).

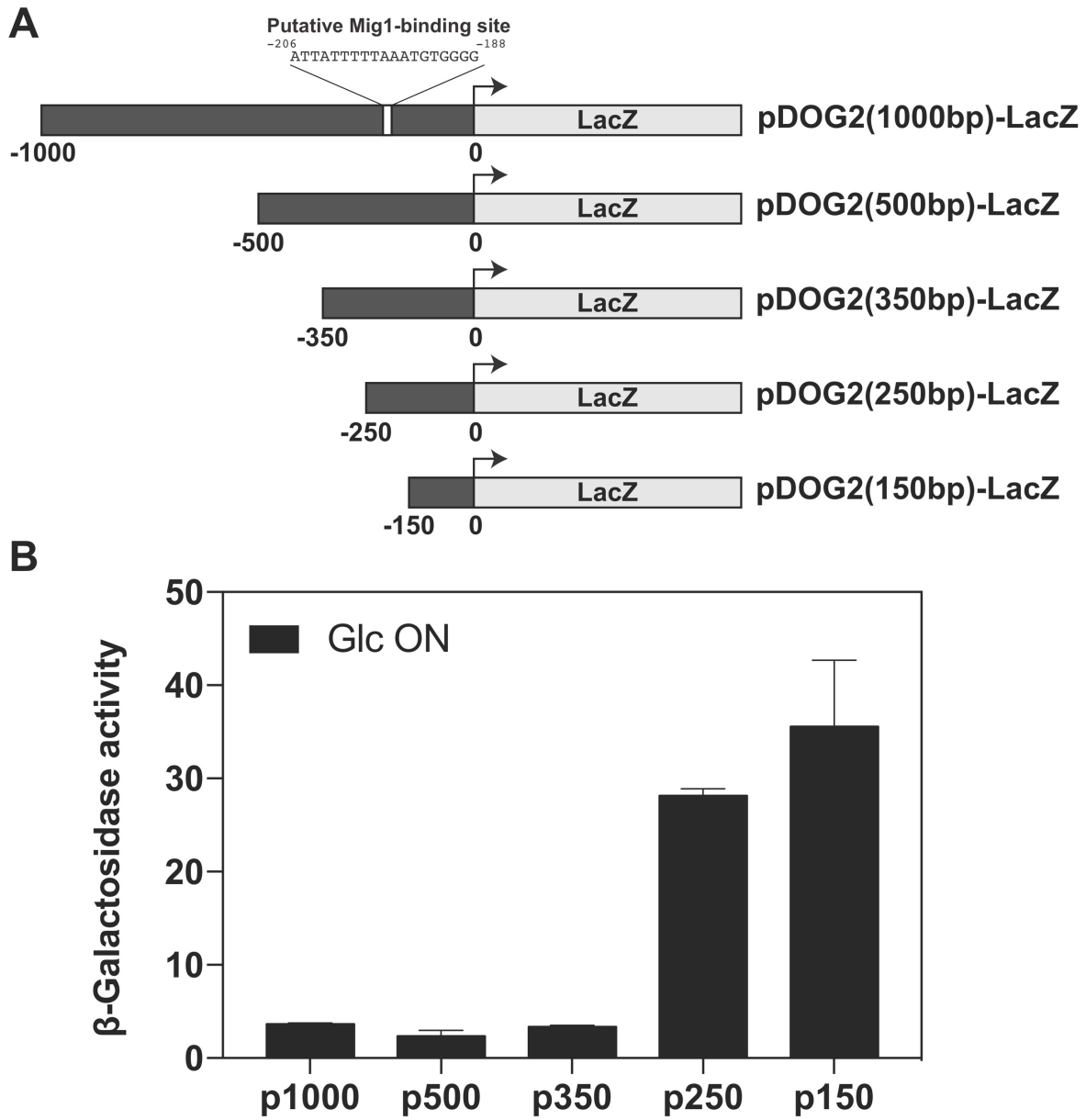

Figure S5. *Cis* regions involved in the regulation of the *DOG2* promoter by glucose
(**A**) Schematic showing the various constructs generated to study *DOG2* promoter regulation by glucose availability. (**B**) β-galactosidase assays on WT cells expressing *LacZ* under the control of the indicated truncated version of the *DOG2* promoter after overnight growth in glucose medium (± SEM, *n*=3 independent experiments, t-test).

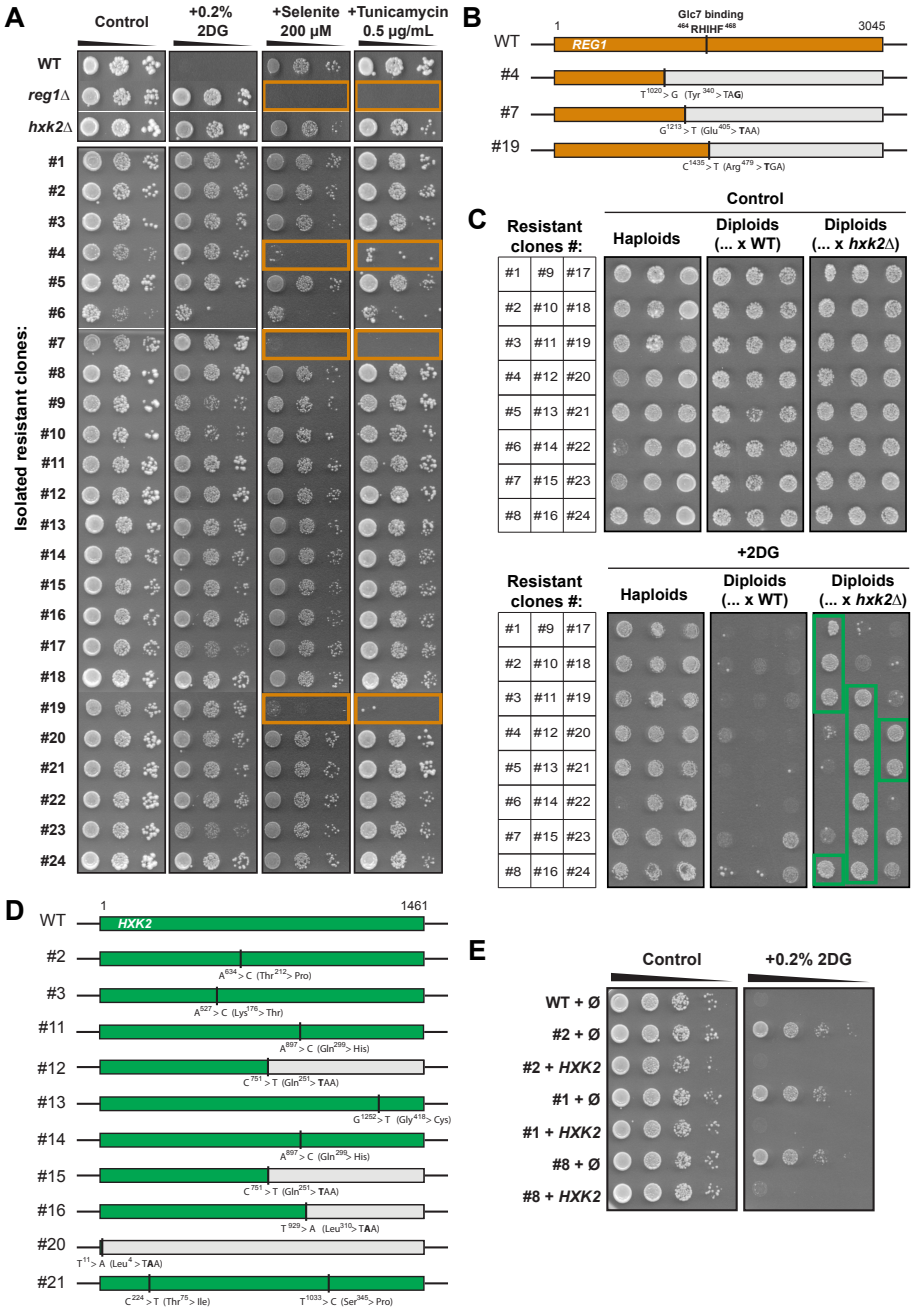

Figure S6. Identification of *reg1* and *hxk2* mutants within the isolated, spontaneous 2DG-resistant mutants

(**A**) Serial dilutions of cultures from the indicated deletion strains and resistant clones were spotted onto SC plates containing no DG or 0.2% 2DG, as well as 200 µM selenite or 0.5 µg/mL tunicamycin and grown for 3 days at 30°C. Note that clone #6 grows very slowly even in absence of 2DG. Orange squares: identified *reg1* mutants. (**B**) Schematic of the identified mutations within the *REG1* ORF in the indicated mutants as obtained by sequencing. (**C**) The 24 resistant clones were crossed with a WT or an *hxk2*Δ strain of the opposite mating type, and cultures of the haploid resistant clones (see matrix, *left*) or the resulting diploids were spotted onto SC medium with or without 0.2% DG. Green squares: identified *hxk2* mutants. (n=2 independent experiments.) (**D**) Schematic of the identified mutations within the *HXK2* ORF in the indicated mutants as obtained by sequencing. (**E**) Growth test showing that the 2DG sensitivity of the 2DG-resistant clones #1 and #8 can be restored by expression of a multicopy, genomic clone containing *HXK2.* Clone #2 (which displays a mutation in *HXK2*, see **D-E**) is used as a positive control. (n=2 independent experiments.)

A

GI	Accession	Description	Species
188497754	NP_000179.2	hexokinase-1 isoform HKI	*Homo sapiens*
410043908	XP_001169264.2	hexokinase-1 isoform 9	*Pan troglodytes*
297301245	XP_001110396.2	hexokinase-1-like isoform 6	*Macaca mulatta*
345798984	XP_536376.3	hexokinase-1 isoform X3	*Canis lupus familiaris*
60592784	NP_001012686.1	hexokinase-1	*Bos taurus*
225735584	NP_001139572.1	hexokinase-1 isoform HK1	*Mus musculus*
6981022	NP_036866.1	hexokinase-1	*Rattus norvegicus*
45383904	NP_989432.1	HK1 gene product	*Gallus gallus*
54606886	NP_998417.1	hexokinase-1	*Danio rerio*
45551986	NP_733151.2	Hex-t2	*Drosophila melanogaster*
17864242	NP_524674.1	hexokinase C	*Drosophila melanogaster*
18079297	NP_524848.1	hexokinase A, isoform	*Drosophila melanogaster*
398364415	NP_116711.3	hexokinase 1	*Saccharomyces cerevisiae S288C*
6321184	**NP_011261.1**	**hexokinase 2**	***Saccharomyces cerevisiae S288C***
50307177	XP_453567.1	KLLA0_D11352g	*Kluyveromyces lactis*
45198797	NP_985826.1	AFR279Cp	*Eremothecium gossypii ATCC 10895*
19113860	NP_592948.1	hexokinase 1	*Schizosaccharomyces pombe*
389624569	XP_003709938.1	hexokinase	*Magnaporthe oryzae 70-15*
164427891	XP_965673.2	hexokinase	*Neurospora crassa OR74A*
15224857	NP_179576.1	hexokinase 2	*Arabidopsis thaliana*
15233457	NP_194642.1	hexokinase 1	*Arabidopsis thaliana*
115464965	NP_001056082.1	Os05g0522500	*Oryza sativa Japonica Group*
115439869	NP_001044214.1	Os01g0742500	*Oryza sativa Japonica Group*
156717322	NP_001096201.1	hexokinase-1	*Xenopus tropicalis*

B

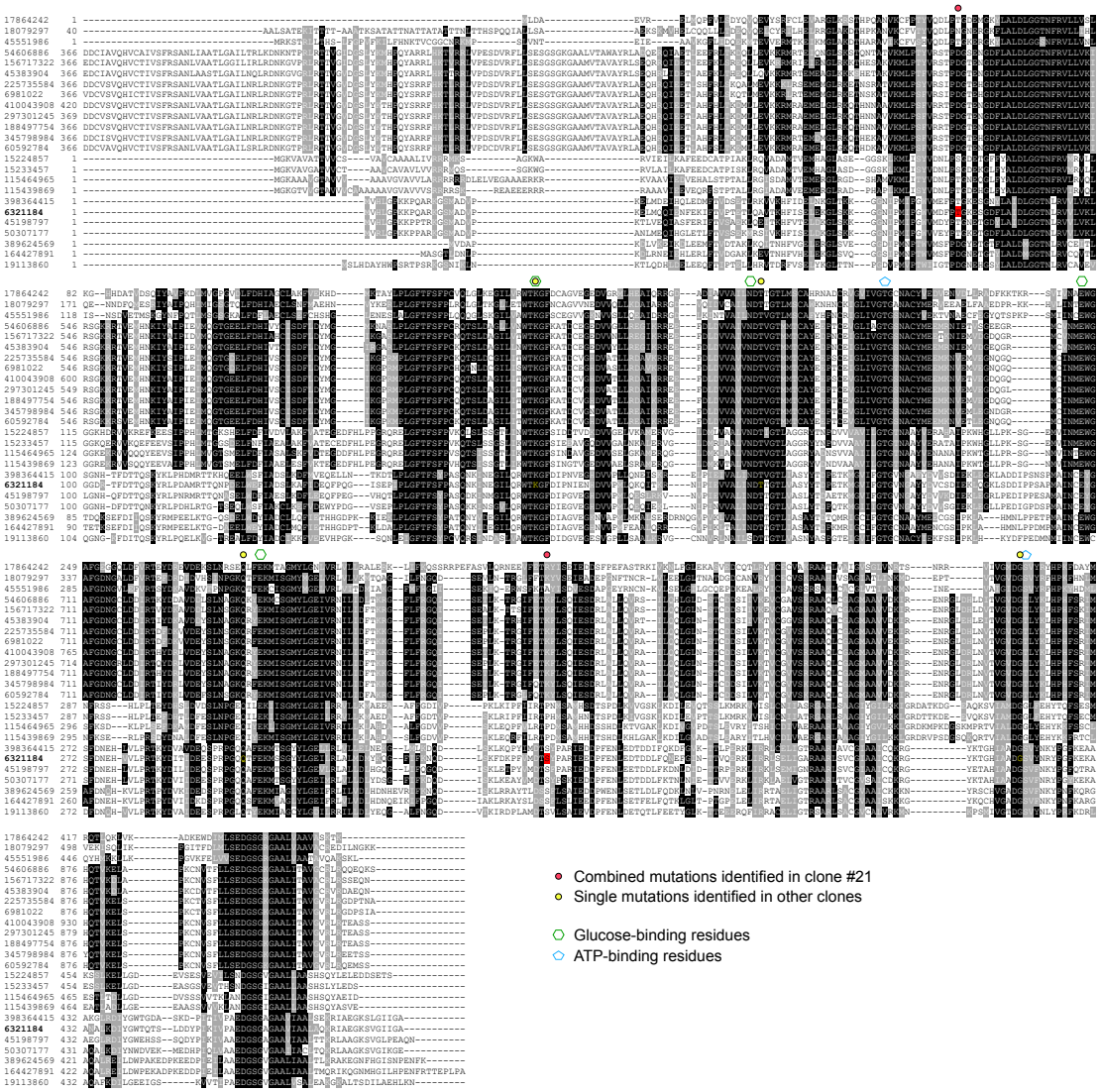

Figure S7. Multiple protein sequence alignment of Hxk2 orthologs and positions of the mutations identified.

(**A**) List of Hxk2 orthologues used for the alignment, as identified using HomoloGene entry #100530 (NCBI). (**B**) The sequences (numbers refer to their GI numbers) were aligned using ClustalX 2.1 (*117*) and formatted using BoxShade server (v.3.21). After the alignment, some sequences were truncated in the N-terminus as indicated. The sequence in bold corresponds to that of *S. cerevisiae* Hxk2.

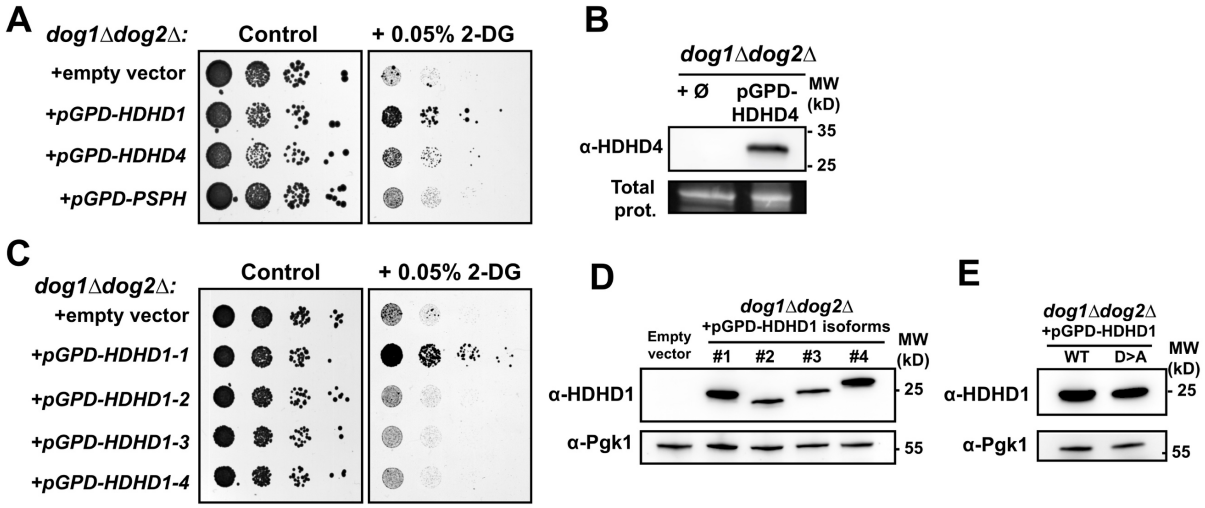

Figure S8. HDHD1 but not its close homologues HDHD4 or PSPH allow resistance to 2DG.
(**A**) Serial dilutions of *dog1*Δ*dog2*Δ strains transformed with the indicated plasmids were spotted on SC-Ura medium with or without 0.05% 2DG and were scanned after 3 days of growth at 30°C. (n=2 independent experiments.) (**B**) Total proteins extracts of *dog1*Δ*dog2*Δ cells transformed with an empty vector or a vector allowing the overexpression of HDHD4 were blotted with an anti-HDHD4 antibody. (n=2 independent experiments.) (**C**) Serial dilutions of *dog1*Δ*dog2*Δ strains transformed with an empty vector or the indicated vectors allowing the expression of the indicated HDHD1 isoforms were spotted on SC-Ura medium with or without 0.05% 2DG and were scanned after 3 days of growth at 30°C. (n=2 independent experiments.) (**D**) Total protein extracts prepared from the same strains as in (**C**) were immunoblotted for HDHD1. Pgk1 (phosphoglycerate kinase) was used as a loading control. (**E**) Total protein extracts prepared from the same strains as in Fig **8C** were immunoblotted for HDHD1. Pgk1 was used as a loading control. (n=2 independent experiments.)

Table S1. Single nucleotide variants in clones #9 and #10 as compared to the WT strain, as identified by whole genome resequencing

Clone	Chrom.	Position	Reference	Mutation	Gene	Mutation in coding region
#9:	chrII	464813	G	A	*CYC8 (YBR112C)*	c.958C>T (p.Gln320X)
	chrXI	570553	C	G	*BET3 (YKR068C)*	c.357G>C (p.Leu119Phe)
	chrXII	969100	C	G	*YLR422W*	c.3204C>G (p.Tyr1068X)
#10	chrII	464813	G	A	*CYC8 (YBR112C)*	c.958C>T (p.Gln320X)
	chrIV	283345	T	A	Intergenic region *GET3-BUG1* (*YDL100C-YDL099W*)	
	chrVIII	303712	T	C	*TRA1 (YHR099W)*	c.952T>C (p.Leu318Leu)
	chrIX	368278	G	C	*PAN1 (YIR006C)*	c.1631C>G (p.Thr544Ser)
	chrXI	570553	C	G	*BET3 (YKR068C)*	c.357G>C (p.Leu119Phe)
	chrXIV	381266	A	C	*DGR1 (YNL130C-A)*	c.126T>G (p.Cys42Trp)
	chrXV	499715	G	A	YOR093C	c.2738C>T (p.Ser913Leu)

Table S2. Yeast strains used in this study.

Name/description	Genotype	Origin/reference	Figures/Panels
BY4741 (WT)	*MATa, ura3Δ0, his3Δ1, leu2Δ0, met15Δ0*	(*118*)	All
ySL2289 Dog1-GFP	*MATa, ura3Δ0, his3Δ1, leu2Δ0, met15Δ0 DOG1::GFP-HIS3MX6*	This study	1C
ySL2290 Dog2-GFP	*MATa, ura3Δ0, his3Δ1, leu2Δ0, met15Δ0 DOG2::GFP-HIS3MX6*	(*103*)	1C, 1G, 1H, 4E
ySL2195 *dog1*Δ	*MATa, ura3Δ0, his3Δ1, leu2Δ0, met15Δ0 dog1Δ::KanMX*	Euroscarf deletion collection	1E
ySL2196 *dog2*Δ	*MATa, ura3Δ0, his3Δ1, leu2Δ0, met15Δ0 dog2Δ::KanMX*	Euroscarf deletion collection	1E, 2J
ySL2197 *dog1*Δ *dog2*Δ	*MATa, ura3Δ0, his3Δ1, leu2Δ0, met15Δ0 dog1Δ-dog2Δ::LEU2MX*	This study	1E, 6B-C, S7A-E
ySL2339 Tdh1-GFP	*MATa, ura3Δ0, his3Δ1, leu2Δ0, met15Δ0 TDH1::GFP-HIS3MX6*	(*103*)	S1
ySL2340 Stf2-GFP	*MATa, ura3Δ0, his3Δ1, leu2Δ0, met15Δ0 STF2::GFP-HIS3MX6*	(*103*)	S1
ySL2341 Eno1-GFP	*MATa, ura3Δ0, his3Δ1, leu2Δ0, met15Δ0 ENO1::GFP-HIS3MX6*	(*103*)	S1
ySL2342 Adh5-GFP	*MATa, ura3Δ0, his3Δ1, leu2Δ0, met15Δ0 ADH5::GFP-HIS3MX6*	(*103*)	S1
ySL2343 Yro2-GFP	*MATa, ura3Δ0, his3Δ1, leu2Δ0, met15Δ0 YRO2::GFP-HIS3MX6*	(*103*)	S1
ySL2344 Hor7-GFP	*MATa, ura3Δ0, his3Δ1, leu2Δ0, met15Δ0 HOR7::GFP-HIS3MX6*	(*103*)	S1
ySL2315 *hog1*Δ	*MATa, ura3Δ0, his3Δ1, leu2Δ0, met15Δ0 hog1Δ::KanMX*	Euroscarf deletion collection	1F, S2A

ySL2416 *hog1*Δ Dog2-GFP	*MATa, ura3Δ0, his3Δ1, leu2Δ0, met15Δ0 hog1Δ::KanMX DOG2::GFP-HIS3MX6*	This study	1G, 1H
ySL2204 *hac1*Δ	*MATa, ura3Δ0, his3Δ1, leu2Δ0, met15Δ0 hac1Δ::KanMX*	This study	2C, 2E-I, 3G, S3B
ySL2205 *ire1*Δ	*MATa, ura3Δ0, his3Δ1, leu2Δ0, met15Δ0 ire1Δ::KanMX*	Euroscarf deletion collection	2H, 2I
ySL567 *snf1*Δ	*MATa, ura3Δ0, his3Δ1, leu2Δ0, met15Δ0 snf1Δ::KanMX*	Euroscarf deletion collection	2H, 4B-D
ySL488 Slt2-GFP	*MATa, ura3Δ0, his3Δ1, leu2Δ0, met15Δ0 SLT2::GFP-HIS3MX6*	(*103*)	S4A
ySL1961 *slt2*Δ	*MATa, ura3Δ0, his3Δ1, leu2Δ0, met15Δ0 slt2Δ::KanMX*	Euroscarf deletion collection	3B-F, S4B-C
ySL557 *wsc1*Δ	*MATa, ura3Δ0, his3Δ1, leu2Δ0, met15Δ0 wsc1Δ::KanMX*	Euroscarf deletion collection	3B
ySL2380 *wsc2*Δ	*MATa, ura3Δ0, his3Δ1, leu2Δ0, met15Δ0 wsc2Δ::KanMX*	Euroscarf deletion collection	3B
ySL2379 *wsc3*Δ	*MATa, ura3Δ0, his3Δ1, leu2Δ0, met15Δ0 wsc3Δ::KanMX*	Euroscarf deletion collection	3B
ySL2386 *mtl1*Δ	*MATa, ura3Δ0, his3Δ1, leu2Δ0, met15Δ0 mtl1Δ::KanMX*	Euroscarf deletion collection	3B
ySL2387 *mid2*Δ	*MATa, ura3Δ0, his3Δ1, leu2Δ0, met15Δ0 mid2Δ::KanMX*	Euroscarf deletion collection	3B
ySL481 *ack1*Δ	*MATa, ura3Δ0, his3Δ1, leu2Δ0, met15Δ0 ack1Δ::KanMX*	Euroscarf deletion collection	3B
ySL2384 *rom1*Δ	*MATa, ura3Δ0, his3Δ1, leu2Δ0, met15Δ0 rom1Δ::KanMX*	Euroscarf deletion collection	3B
ySL590 *rom2*Δ	*MATa, ura3Δ0, his3Δ1, leu2Δ0, met15Δ0 rom2Δ::KanMX*	Euroscarf deletion collection	3B
ySL2385 *tus1*Δ	*MATa, ura3Δ0, his3Δ1, leu2Δ0, met15Δ0 tus1Δ::KanMX*	Euroscarf deletion collection	3B
ySL2405 *bck1*Δ	*MATa, ura3Δ0, his3Δ1, leu2Δ0, met15Δ0 bck1Δ::KanMX*	Euroscarf deletion collection	3B, 3F
ySL2382 *mkk1*Δ	*MATa, ura3Δ0, his3Δ1, leu2Δ0, met15Δ0 mkk1Δ::KanMX*	Euroscarf deletion collection	3B
ySL2383 *mkk2*Δ	*MATa, ura3Δ0, his3Δ1, leu2Δ0, met15Δ0 mkk2Δ::KanMX*	Euroscarf deletion collection	3B
ySL2381 *rlm1*Δ	*MATa, ura3Δ0, his3Δ1, leu2Δ0, met15Δ0 rlm1Δ::KanMX*	Euroscarf deletion collection	3B
ySL2297 Dog1-TAP Dog2-GFP	*MATa, ura3Δ0, his3Δ1, leu2Δ0, met15Δ0 DOG1::TAP-KanMX, DOG2::GFP-HIS3MX6*	This study	4B
ySL2298 Dog1-TAP Dog2-GFP *snf1*Δ	*MATa, ura3Δ0, his3Δ1, leu2Δ0, met15Δ0 DOG1::TAP-KanMX, DOG2::GFP-HIS3MX6, snf1Δ::hphNT1*	This study	4B
ySL2292 Dog2-GFP *mig1*Δ	*MATa, ura3Δ0, his3Δ1, leu2Δ0, met15Δ0 DOG2::GFP-HIS3MX6, mig1Δ::KanMX*	This study	4F
ySL2293 Dog2-GFP *mig2*Δ	*MATa, ura3Δ0, his3Δ1, leu2Δ0, met15Δ0 DOG2::GFP-HIS3MX6, mig2Δ::KanMX*	This study	4F

ySL2294 Dog2-GFP *mig1*Δ *mig2*Δ	*MATa, ura3Δ0, his3Δ1, leu2Δ0, met15Δ0 DOG2::GFP-HIS3MX6, mig1Δ::LEU2MX, mig2Δ::KanMX*	This study	4F
ySL2295 Dog2-GFP *hxk2*Δ	*MATa, ura3Δ0, his3Δ1, leu2Δ0, met15Δ0 DOG2::GFP-HIS3MX6, hxk2Δ::KanMX*	This study	4F
ySL2291 Dog2-GFP *reg1*Δ	*MATa, ura3Δ0, his3Δ1, leu2Δ0, met15Δ0 DOG2::GFP-HIS3MX6, reg1Δ::LEU2MX*	This study	4F
ySL2192 *mig1*Δ	*MATa, ura3Δ0, his3Δ1, leu2Δ0, met15Δ0 mig1Δ::KanMX*	Euroscarf deletion collection	4E
ySL2193 *mig2*Δ	*MATa, ura3Δ0, his3Δ1, leu2Δ0, met15Δ0 mig2Δ::KanMX*	Euroscarf deletion collection	4E
ySL2194 *mig1*Δ *mig2*Δ	*MATa, ura3Δ0, his3Δ1, leu2Δ0, met15Δ0 mig1Δ::KanMX, mig2Δ::HIS3MX6*	This study	4E, 4G
ySL2200 *hxk2*Δ	*MATa, ura3Δ0, his3Δ1, leu2Δ0, met15Δ0 hxk2Δ::KanMX*	Euroscarf deletion collection	4E, 4G, 5B
ySL2447 *hxk2*Δ	*MATalpha, ura3Δ0, his3Δ1, leu2Δ0, met15Δ0 hxk2Δ::KanMX*	Euroscarf deletion collection	5D
ySL2199 *reg1*Δ	*MATa, ura3Δ0, his3Δ1, leu2Δ0, met15Δ0 reg1Δ::HIS3MX6*	This study	4E, 4G, 5C, S6A
ySL2201 *reg1*Δ *dog1*Δ *dog2*Δ	*MATa, ura3Δ0, his3Δ1, leu2Δ0, met15Δ0 reg1Δ::HIS3MX6, dog1Δ-dog2Δ::LEU2MX*	This study	4G
ySL2202 *hxk2*Δ *dog1*Δ *dog2*Δ	*MATa, ura3Δ0, his3Δ1, leu2Δ0, met15Δ0 hxk2Δ::KanMX, dog1Δ-dog2Δ::LEU2MX*	This study	4G
ySL2203 *mig1*Δ *mig2*Δ *dog1*Δ *dog2*Δ	*MATa, ura3Δ0, his3Δ1, leu2Δ0, met15Δ0 mig1Δ::KanMX, mig2Δ::HIS3MX6, dog1Δ-dog2Δ::LEU2MX*	This study	4G
ySL2317 *mig1*Δ *mig2*Δ *snf1*Δ	*MATa, ura3Δ0, his3Δ1, leu2Δ0, met15Δ0 mig1Δ::KanMX, mig2Δ::HIS3MX6, snf1Δ::NatMX*	This study	4G
ySL2474 mut. #9	Spontaneous mutant arising from BY4741 strain (*MATa, ura3Δ0, his3Δ1, leu2Δ0, met15Δ0*) selected on 0.2% 2DG	This study	5A, 5C-F, S6A
ySL2475 mut. #10	Spontaneous mutant arising from BY4741 strain (*MATa, ura3Δ0, his3Δ1, leu2Δ0, met15Δ0*) selected on 0.2% 2DG	This study	5A, 5C-F, S6A
ySL2476 mut. #9-Dog2-GFP	ySL2474 *DOG2::GFP- HIS3MX6*	This study	5F-G
ySL2477 mut. #10-Dog2-GFP	ySL2475 *DOG2::GFP- HIS3MX6*	This study	5F-G
ySL2614 mut. #9-*dog1*Δ *dog2*Δ	ySL2474 *dog1Δ-dog2Δ::HphNT1*	This study	5H
ySL2615 mut. #10-*dog1*Δ *dog2*Δ	ySL2475 *dog1Δ-dog2Δ::HphNT1*	This study	5H

Table S3. Plasmids used in this study.

Name	Description	Origin/reference
pSL209	pGP564: empty vector control for genomic tiling collection, 2µ, *LEU2*	(*119*)
pSL409	p_{DOG1}(1000bp):*lacZ*, 2µ, *URA3* (Yep58-based)	This study
pSL410	p_{DOG2}(1000bp):*lacZ*, 2µ, *URA3* (Yep58-based)	This study
pSL405	p_{UPRE1}:*lacZ*, 2µ, *URA3* (pGA1695-based)	P. Walter's lab, pJC5 (*52*)
pSL385	$p_{CYC(2xRlm1)}$:*lacZ* , 2µ, *URA3* (pLGΔ-312-based)	D. Levin's lab, p1434 (*120*)
pSL412	p_{GPD}:*DOG2*, 2µ, *URA3* (pRS426-based)	This study
pSL425	pGP564-based genomic clone YGPM10o10 containing *DOG1* and *DOG2*; 2µ, *LEU2* (genomic tiling collection - chr.VIII:188052-198738)	(*119*)
pSL438	p_{DOG2}(150bp):*lacZ*, 2µ, *URA3* (Yep58-based)	This study
pSL439	p_{DOG2}(250bp):*lacZ*, 2µ, *URA3* (Yep58-based)	This study
pSL440	p_{DOG2} (350bp):*lacZ*, 2µ, *URA3* (Yep58-based)	This study
pSL441	p_{DOG2} (500bp):*lacZ*, 2µ, *URA3* (Yep58-based)	This study
pSL411	p_{GPD}:*DOG1*, 2µ, *URA3* (pRS426-based)	This study
pSL413	p_{GPD}:*yniC*, 2µ, *URA3* (pRS426-based)	This study
pSL414	p_{GPD}:*HDHD1-isoform 1*, 2µ, *URA3* (pRS426-based)	This study
pSL492	p_{GPD}:*HDHD1-isoform 2*, 2µ, *URA3* (pRS426-based)	This study
pSL493	p_{GPD}:*HDHD1-isoform 3*, 2µ, *URA3* (pRS426-based)	This study
pSL494	p_{GPD}:*HDHD1-isoform 4*, 2µ, *URA3* (pRS426-based)	This study
pSL495	p_{GPD}:*HDHD4*, 2µ, *URA3* (pRS426-based)	This study
pSL496	p_{GPD}:*PSPH*, 2µ, *URA3* (pRS426-based)	This study
ySL2335	p_{GPD}:*HDHD1-isoform 1-DD>AA*, 2µ, *URA3* (pRS426-based)	This study
pSL422	*pCMV-SPORT6-HDHD1*	Dharmacon (CloneId:4478358)
pSL458	*pCS2* (empty vector - expression in mammalian cells)	(*121*)
pSL431	*pET15b-6His-HDHD1*	E. van Schaftigen (*83*)
pSL459	*pET15b-6His-HDHD1(DD>AA)*	This study
pSL460	pGP564-based genomic clone YGPM24j02 containing *HXK2*; 2µ, *LEU2* (genomic tiling collection - chr.VII: 23019-35747)	(*119*)
pSL465	pGP564-based genomic clone YGPM2h11 containing *CYC8*; 2µ, *LEU2* (genomic tiling collection - chr. II: 458726-473023)	(*119*)
pSL466	*CYC8* (-1000/+300) ; CEN, *LEU2* (pRS415-based)	This study
pSL467	*cyc8*(C^{958}>T) (-1000/+300) ; CEN, *LEU2* (pRS415-based)	This study

Table S4. Antibodies used in this study.

Name	Description	Dilution	Reference/Origin
α GFP	Mouse monoclonal against GFP, clones 7.1 and 13.1	1/5000	11814460001 - Roche
α Rsp5/Nedd4	Rabbit polyclonal antibody against Nedd4	1/5000	ab14592 - Abcam
α Ⓟp38/ⓅHog1	Mouse monoclonal against Tyr182-phosphorylated p38 (E-1)	1/1000	sc166182 - Santa Cruz
α p38/Hog1	Mouse monoclonal against human p38 (D-3)	1/1000	sc165978 -Santa Cruz
α CPY	Rabbit polyclonal against Carboxypeptidase Y (PRC1)	1/2000	ab34636 - Abcam
PAP	Peroxidase-anti-Peroxidase complex	1/5000	P1291-Sigma Aldrich
α ⓅAMPK/ⓅSnf1	Rabbit polyclonal against Thr172-phosphorylated human AMPKα	1/1000	#2535 –Cell Signaling Technology
α Ⓟ p44/42 MAPK (Erk1/2) (T202/Y204)	Rabbit monoclonal against a synthetic phosphopeptide corresponding to residues surrounding Thr202/Tyr204 of human p44 MAP kinase	1/2000	#4370 - Cell Signaling Technology
α polyHis tag	Mouse monoclonal antibody used to reveal endogenous Snf1 which contains a stretch of 13 His residues	1/2000	# H1029 - Sigma
α HDHD1	Rabbit polyclonal against human HDHD1. To visualize HDHD1 in lysates of yeast or bacteria overexpressing HDHD1.	1/2000	SAB2700505 - Sigma
α HDHD4	Mouse monoclonal anti-HDHD4 (NANP) Antibody (D8). To visualize HDHD4 in lysates of yeast overexpressing HDHD4.	1/5000	sc-374637-Santa Cruz
α-CD147	Mouse monoclonal anti-CD147 (Clone HIM6)	1/5000	555961-BD Bioscience
α-PGK	Rabbit polyclonal against yeast 3-phosphoglycerate kinase	1/10000	NE130/7S Nordic MUBio
α -Suc2 (invertase)	Rabbit polyclonal against invertase	1/5000	C. Stirling
α Rabbit IgG	Goat secondary antibody against Rabbit IgG	1/5000	A6154 - Sigma Aldrich
α Mouse IgG	Goat secondary antibody against Mouse IgG	1/5000	A5278 - Sigma Aldrich

Data File S1. Proteomic response to 2DG treatment.